fractal and fractional

MDPI

Article

Time-Varying Function Matrix Projection Synchronization of Caputo Fractional-Order Uncertain Memristive Neural Networks with Multiple Delays via Mixed Open Loop Feedback Control and Impulsive Control

Hongguang Fan [1,2,3], Yue Rao [1], Kaibo Shi [4] and Hui Wen [5,*]

[1] College of Computer, Chengdu University, Chengdu 610106, China; fanhongguang@cdu.edu.cn (H.F.); raoyue@stu.cdu.edu.cn (Y.R.)
[2] Engineering Research Center of Big Data Application in Private Health Medicine, Fujian Province University, Putian 351100, China
[3] School of Mathematical and Computational Science, Hunan University of Science and Technology, Xiangtan 411201, China
[4] School of Electronic Information and Electrical Engineering, Chengdu University, Chengdu 610106, China; shikaibo@cdu.edu.cn
[5] New Engineering Industry College, Putian University, Putian 351100, China
* Correspondence: wen_hui81@ptu.edu.cn

Abstract: This paper shows solicitude for the generalized projective synchronization of Caputo fractional-order uncertain memristive neural networks (FOUMNNs) with multiple delays. By extending the constant scale factor to the time-varying function matrix, we establish an extraordinary synchronization mode called time-varying function matrix projection synchronization (TFMPS), which is a generalized version of traditional matrix projection synchronization, modified projection synchronization, complete synchronization, and anti-synchronization. To achieve the goal of TFMPS, we design a novel mixed controller including the open loop feedback control and impulsive control, which employs the state information in the time-delayed interval and the sampling information at the impulse instants. It has a prominent advantage that impulse intervals are not restricted by time delays. To establish the connection between the error system and the auxiliary system, a generalized fractional-order comparison theorem with time-varying coefficients and impulses is established. Applying the stability theory, the comparison theorem, and the Laplace transform, new synchronization criteria of FOUMNNs are acquired under the mixed impulsive control schemes, and the derived synchronization theorem and corollary can effectively expand the correlative synchronization achievements of fractional-order systems.

Keywords: fractional-order; neural networks; mixed control; impulsive sampling; synchronization

Citation: Fan, H.; Rao, Y.; Shi, K.; Wen, H. Time-Varying Function Matrix Projection Synchronization of Caputo Fractional-Order Uncertain Memristive Neural Networks with Multiple Delays via Mixed Open Loop Feedback Control and Impulsive Control. *Fractal Fract.* **2024**, *8*, 301. https://doi.org/10.3390/fractalfract8050301

Academic Editor: Norbert Herencsar

Received: 16 April 2024
Revised: 11 May 2024
Accepted: 16 May 2024
Published: 20 May 2024

1. Introduction

Neural networks can simulate the thinking process of the human brain and have important application value in the field of artificial intelligence [1]. With the rise of intelligent computing, various interdisciplinary fields such as machine learning, control theory, computer science, and system stability require neural networks as important research tools [2–9]. Memristors, as the fourth basic circuit component, have a monumental memory function similar to the neuronal protrusions in the human brain [10]. They can be stored and calculated in a cross-array form, with fast computing speed and low energy consumption when processing analog signals. The research results have shown that using memristors to replace neuronal protrusions can establish various memristive neural networks with parallel computing capabilities [11]. Therefore, memristive neural networks (MNNs), as a special type of state-dependent network model, naturally receive much attention from scientific research personnel [12–14].

Due to the nonlinear nature of memristor-based neural networks, MNNs are often rich in dynamic states, such as equilibrium points, periodic solutions, traveling wave solutions, synchronization, and chaos. Applying integer-order differential integral operators to model the network dynamic behaviors, memristor-based neural networks have been widely studied [15]. In particular, synchronization, as an important stable state in neural networks, can be achieved through internal coupling or external force input [16]. For instance, utilizing external non-delayed and delayed impulse effects, the authors in [17] deliberated the global synchronization task of stochastic MNNs with Wiener distribution and coupling delays. Based on the differential inclusions, Li et al. [18] paid attention to the synchronization within a settling time for master-slave MNNs involving nonlinear driving functions and variable system delays using adaptive feedback schemes. In [19], the authors solved the fixed-time driver-response synchronization challenge of MNNs including complex-valued parameters. In [20], Alsaedi et al. deliberated the complete synchronization of fuzzy MNNs with external perturbation by using fuzzy rules and adaptive rules. In [21], Fu et al. dealt with the weak projective synchronization task for Takagi-Sugeno fuzzy MNNs with parameter mismatch based on Liapunov-Krasovsky functions and variable parameter formulas.

The synchronization research results of MNNs mentioned above mainly focused on mathematical modeling based on integer-order calculus operators. Fractional calculus, as a promotional version of integer order differentiation and integration, adds a degree of freedom parameter, and more importantly, includes all the communication from the initial moment to the current one [22]. Therefore, it has special memory and heritability, which can characterize various phenomena and processes that cannot be described by integer calculus [23]. As a simple example, in neural cell tissues, the application of fractional calculus can break the inherent complexity of a single molecular membrane, thereby comprehensively understanding the memory capability and behavior of biological systems. Researchers replaced ordinary capacitors with fractional capacitors and established the fractional-order memristive neural network model, which can better characterize the function and behavior of neurons. In [24], using the nature of the proportional derivative, a class of generalized Caputo and Riemann-Liouville fractional derivatives including exponential kernels was studied. In [25], utilizing stability theory and immovable point techniques, the solution of proportional Liouville-Caputo fractional stochastic equations was discussed. By introducing the Riemann-Liouville fractional derivative, Gu et al. [26] established fractional-order MNNs with unsuspected parameters, and further implemented parameter adaptive discrimination and identification. With the help of the Caputo fractional derivative, Chen et al. [27] constructed fractional-order Caputo MNNs and analyzed the global stability conditions of the system in detail. Li et al. [28] studied the nonlocal anti-synchronization challenge for fractional-order neural networks involving mixed variable delays utilizing state information feedback. Yang et al. [29] deliberated the complete synchronization for fractional-order delayed MNNs with unidentified parameters by feedback control schemes. More synchronization results, such as robust synchronization [30] and pinning multi-synchronization [31] for fractional-order MNNs were investigated based on fractional-order Lyapunov function methods.

In particular, two complex systems are known to achieve projective synchronization if the corresponding state variables of master neural networks and slave neural networks reach identical dynamical behavior under certain scaling factors [32]. Projection synchronization can be regarded as a generalized class of synchronization modes since it can be converted into synchronization modes such as complete synchronization and anti-synchronization by adjusting the projection scaling factor. Note that projection synchronization can be relied upon for faster communication with its scaling properties [33]. Consequently, it has important theoretical and practical significance to investigate the projection synchronization of fractional-order neural networks. Latterly, researchers used different control strategies to solve the projective synchronization goal for fractional-order MNNs, and many worthwhile works have been achieved [34–40]. For instance, in [34],

Velmurugan et al. dealt with the hybrid projection synchronization of fractional-order MNNs with delays based on a simple state feedback control scheme. Gu et al. [35] discussed the projection synchronization of fractional-order delayed MNNs by applying open-loop control and continuous feedback control. Considering the sliding mode control and adaptive control techniques, researchers in [36] investigated the passive projective synchronization of uncertain MNNs and derived the stability conditions for error systems. In [37,38], the projection synchronization and the modified projection synchronization of fractional-order MNNs in finite time were explored based on feedback control methods. Ding et al. [40] were concerned about the complex projection synchronization for fractional-order complex-valued MNNs utilizing hybrid feedback controllers.

As everyone knows, the scale factor in projection synchronization as a key parameter increases the safety of signal transmission between the drive and response systems. However, as mentioned above in the literature [34–40], the projected scale factors between fractional-order master-slave networks are generally constant matrices or fixed diagonal forms. If the scale factor is adjusted to be a time-varying function matrix including multiple variable elements, it undoubtedly increases the communication security letter. Until now, no works have considered projective synchronization with scaling factors of time-varying function matrices for FOUMNNs by mixed impulsive feedback control. This is also the main motivation of this study. The main reasons include three points. First, scaling factors that vary with time t are more complex to predict than constant matrices or fixed diagonal forms. Second, the delays or uncertainties caused by limited information processing speed or external disturbances can make the dynamic behaviors of the system more complex and disrupt the stability of nonlinear systems. Third, the primary objective of this study is to develop a broader projection synchronization model and to overcome the previously mentioned difficulties with a new mixed impulsive feedback control technique. This requires us to establish a more generalized impulse comparison theorem first.

Motivated by what has been considered above, this article deliberates the TFMPS of Caputo FOUMNNs with multiple delays. The worthwhile contributions of this study include three aspects. First, we extend the traditional projective scaling factor to a time-dependent function matrix and define a generalized synchronization mode, i.e., TFMPS. This synchronization mode can degenerate into matrix projective synchronization (PS) [41], modified PS [38], and anti-synchronization under specific restrictive requirements. The adjustability of fractional orders and the time-varying unpredictability of elements in function matrices can improve the safety of secret communication, providing better application prospects for communication encryption systems. Second, an important impulsive comparison theorem that considers delays and time-varying coefficients is provided as an analytical tool. In addition to the memristive neural network model considered in this article, the comparison theorem can be applied to more neural networks, such as pantograph neural networks or Cohen-Grossberg neural networks. Finally, different from the feedback control or sliding mode control schemes in [34–40], novel mixed impulsive feedback control schemes, including open-loop feedback control and impulsive sampling control, have been designed to achieve the TFMPS in FOUMNNs. Both the state information in the time-delayed interval and the sampling information at the impulse moments are comprehensively utilized in our controller. Theoretical analysis and numerical experiments show that the derived synchronization conditions rely on impulsive strengths, feedback strengths, uncertain boundaries, and fractional order.

2. Theoretical Foundation and Model Establishment

In this section, some fundamental knowledge closely related to this study is first reviewed. Then, an important impulsive comparison theorem involving various delays is given, and drive-response network models concerning the Caputo derivative are established.

Definition 1 ([34]). *Fractional integral for an integral function $\mathcal{F}(t)$ is given as*

$$I_t^{\eta}\mathcal{F}(t) = \frac{1}{\Gamma(\eta)}\int_{t_0}^{t}(t-\varsigma)^{\eta-1}\mathcal{F}(\varsigma)d\varsigma, \tag{1}$$

where $t \geq t_0$, $\eta > 0$, and $\Gamma(\eta) = \int_0^{+\infty} t^{\eta-1}e^{-t}dt$.

Definition 2 ([34]). *η-order Caputo derivative for a function $\mathcal{F}(t)$ is given by*

$${}^{c}D_t^{\eta}\mathcal{F}(t) = \frac{1}{\Gamma(m-\eta)}\int_{t_0}^{t}(t-\varsigma)^{m-\eta-1}\mathcal{F}^{(m)}(\varsigma)d\varsigma, \tag{2}$$

where $t \geq t_0$, and $0 \leq m-1 < \eta < m$. Especially, when $0 < \eta < 1$, ${}^{c}D_t^{\eta}\mathcal{F}(t) = \frac{1}{\Gamma(1-\eta)}\int_{t_0}^{t}(t-\varsigma)^{-\eta}\mathcal{F}'(\varsigma)d\varsigma$; when $\eta = 1$, the fractional derivative ${}^{c}D_t^{\eta}\mathcal{F}(t)$ can convert to the one-order derivative.

Consider fractional-order uncertain memristive neural networks involving multiple delays as below:

$$\begin{aligned}{}^{c}D_t^{\eta}p_k(t) = &-w_k p_k(t) + \sum_{j=1}^{n}\Big(u_{kj}(p_j(t)) + \Delta\overline{u}_{kj}(t)\Big)\phi_j(p_j(t)) + \sum_{j=1}^{n}\Big(v_{kj}(p_j(t))\\ &+ \Delta\overline{v}_{kj}(t)\Big)\varphi_j(p_j(t-\tau_j)) + I_k(t),\ k = 1,2,\cdots,n,\ t \geq 0,\end{aligned} \tag{3}$$

where $\eta \in (0,1)$ and w_k is a positive parameter signifying the decay rate coefficient. τ_j denotes the jth transmission delay satisfying $0 \leq \tau_j \leq \tau$. $I_k(t)$ represents the bounded control input. $p(t) = (p_1(t), p_2(t), \cdots, p_n(t))^T$ stands for the state vector at point t. $\phi_j(p_j(t))$ and $\varphi_j(p_j(t-\tau_j))$ mean nonlinear activation functions at points t and $t-\tau_j$, respectively. $\Delta\overline{u}_{kj}(t)$ and $\Delta\overline{v}_{kj}(t)$ express the uncertain deviation of $u_{kj}(p_j(t))$ and $v_{kj}(p_j(t))$, which satisfying $|\Delta\overline{u}_{kj}(t)| \leq \rho_{kj}$ and $|\Delta\overline{v}_{kj}(t)| \leq \varrho_{kj}$. The initial conditions of memristive system (3) are $p(s) = \varsigma(s) = (\varsigma_1(s), \varsigma_2(s), \cdots, \varsigma_n(s))^T \in \mathbb{C}([-\tau, 0], \mathbb{R}^n)$. $u_{kj}(p_j(t))$ and $v_{kj}(p_j(t))$ represent the connection weights, where

$$u_{kj}(p_j(t)) = \frac{W_{kj}}{C_k} \times SIGN_{kj},\ v_{kj}(p_j(t)) = \frac{M_{kj}}{C_k} \times SIGN_{kj},\ SIGN_{kj} = \begin{cases}1, & k \neq j,\\ -1, & k = j.\end{cases} \tag{4}$$

W_{kj} and M_{kj} describe the memductances of resistors $\tilde{W}_{kj}$ and $\tilde{M}_{kj}$. $\tilde{W}_{kj}$ displays the resistor between $\phi_j(p_j(t))$ and $p_k(t)$. $\tilde{M}_{kj}$ displays the resistor between $\varphi_j(p_j(t-\tau_j))$ and $p_k(t)$. C_k represents the voltage of the capacitor. Considering the distinctions of the memristor and the nature of current-voltage, $u_{kj}(p_j(t))$ and $v_{kj}(p_j(t))$ satisfy two constraints as follows:

$$u_{kj}(p_j(t)) = \begin{cases}u_{kj}^{*}, & |p_j(t)| < X_j,\\ u_{kj}^{**}, & |p_j(t)| > X_j,\end{cases}\quad v_{kj}(p_j(t)) = \begin{cases}v_{kj}^{*}, & |p_j(t)| < X_j,\\ v_{kj}^{**}, & |p_j(t)| > X_j,\end{cases} \tag{5}$$

where $k, j = 1,2,\cdots,n$, $u_{kj}(\pm X_j) = u_{kj}^{*}$ or u_{kj}^{**}, $v_{kj}(\pm X_j) = v_{kj}^{*}$ or v_{kj}^{**}, and the switching jumps $X_j > 0$. $u_{kj}^{*}, u_{kj}^{**}, v_{kj}^{*}$, and v_{kj}^{**} are scalars regarding memristances.

By manipulating the differential inclusion theory, uncertain memristive dynamical networks (3) are reformulated as

$$\begin{aligned}{}^{c}D_t^{\eta}p_k(t) \in &-w_k p_k(t) + \sum_{j=1}^{n}\Big(co(\underline{u}_{kj}, \overline{u}_{kj}) + \Delta\overline{u}_{kj}(t)\Big)\phi_j(p_j(t)) + \sum_{j=1}^{n}\Big(co(\underline{v}_{kj}, \overline{v}_{kj})\\ &+ \Delta\overline{v}_{kj}(t)\Big)\varphi_j(p_j(t-\tau_j)) + I_k(t),\ k = 1,2,\cdots,n,\ t \geq 0,\end{aligned} \tag{6}$$

where $\underline{u}_{kj} = \min\{u^*_{kj}, u^{**}_{kj}\}$, $\overline{u}_{kj} = \max\{u^*_{kj}, u^{**}_{kj}\}$, $\underline{v}_{kj} = \min\{v^*_{kj}, v^{**}_{kj}\}$, $\overline{v}_{kj} = \max\{v^*_{kj}, v^{**}_{kj}\}$, $u^+_{kj} = \max\{|\underline{u}_{kj}|, |\overline{u}_{kj}|\}$, $v^+_{kj} = \max\{|\underline{v}_{kj}|, |\overline{v}_{kj}|\}$,

$$co(\underline{u}_{kj}, \overline{u}_{kj}) = \begin{cases} u^*_{kj}, & |p_j(t)| < X_j, \\ co(\underline{u}_{kj}, \overline{u}_{kj}), & |p_j(t)| = X_j, \\ u^{**}_{kj}, & |p_j(t)| > X_j, \end{cases} \quad co(\underline{v}_{kj}, \overline{v}_{kj}) = \begin{cases} v^*_{kj}, & |p_j(t)| < X_j, \\ co(\underline{v}_{kj}, \overline{v}_{kj}), & |p_j(t)| = X_j, \\ v^{**}_{kj}, & |p_j(t)| > X_j, \end{cases}$$

then, there exist functions $\xi_{kj}(t) \in co(\underline{u}_{kj}, \overline{u}_{kj})$, $\zeta_{kj}(t) \in co(\underline{v}_{kj}, \overline{v}_{kj})$, for $k, j = 1, 2, \cdots, n$, such that

$$\begin{aligned} {}^cD^\eta_t p_k(t) = &- w_k p_k(t) + \sum_{j=1}^{n} \Big(\xi_{kj}(t) + \Delta\overline{u}_{kj}(t)\Big)\phi_j(p_j(t)) + \sum_{j=1}^{n} \Big(\zeta_{kj}(t) \\ &+ \Delta\overline{v}_{kj}(t)\Big)\varphi_j(p_j(t-\tau_j)) + I_k(t),\ k = 1, 2, \cdots, n,\ t \geq 0. \end{aligned} \tag{7}$$

Based on neural networks (3), one can obtain the corresponding response networks as below:

$$\begin{aligned} {}^cD^\eta_t q_k(t) = &- w_k q_k(t) + \sum_{j=1}^{n} \Big(u_{kj}(q_j(t)) + \Delta\overline{u}_{kj}(t)\Big)\phi_j(q_j(t)) + \sum_{j=1}^{n} \Big(v_{kj}(q_j(t)) \\ &+ \Delta\overline{v}_{kj}(t)\Big)\varphi_j(q_j(t-\tau_j)) + I_k(t) + U_k(t),\ k = 1, 2, \cdots, n,\ t \geq 0, \end{aligned} \tag{8}$$

where $U_k(t)$ is the mixed impulsive feedback controller. The initial conditions of response memristive networks (8) are $q(s) = \xi(s) = (\xi_1(s), \xi_2(s), \cdots, \xi_n(s))^T \in \mathbb{C}([-\tau, 0], \mathbb{R}^n)$. $u_{kj}(q_j(t))$ and $v_{kj}(q_j(t))$ represent the connection weights and can be defined by

$$u_{kj}(q_j(t)) = \begin{cases} u^*_{kj}, & |q_j(t)| < X_j, \\ u^{**}_{kj}, & |q_j(t)| > X_j, \end{cases} \quad v_{kj}(q_j(t)) = \begin{cases} v^*_{kj}, & |q_j(t)| < X_j, \\ v^{**}_{kj}, & |q_j(t)| > X_j, \end{cases}$$

where $k, j = 1, 2, \cdots, n$, and the switching jumps $X_j > 0$. $u^*_{kj}, u^{**}_{kj}, v^*_{kj}$, and v^{**}_{kj} are constants. Then, memristive networks (8) can be rewritten by

$$\begin{aligned} {}^cD^\eta_t q_k(t) \in &- w_k q_k(t) + \sum_{j=1}^{n} \Big(co(\underline{u}_{kj}, \overline{u}_{kj}) + \Delta\overline{u}_{kj}(t)\Big)\phi_j(q_j(t)) + \sum_{j=1}^{n} \Big(co(\underline{v}_{kj}, \overline{v}_{kj}) \\ &+ \Delta\overline{v}_{kj}(t)\Big)\varphi_j(q_j(t-\tau_j)) + I_k(t) + U_k(t),\ k = 1, 2, \cdots, n,\ t \geq 0, \end{aligned} \tag{9}$$

where

$$co(\underline{u}_{kj}, \overline{u}_{kj}) = \begin{cases} u^*_{kj}, & |q_j(t)| < X_j, \\ co(\underline{u}_{kj}, \overline{u}_{kj}), & |q_j(t)| = X_j, \\ u^{**}_{kj}, & |q_j(t)| > X_j, \end{cases} \quad co(\underline{v}_{kj}, \overline{v}_{kj}) = \begin{cases} v^*_{kj}, & |q_j(t)| < X_j, \\ co(\underline{v}_{kj}, \overline{v}_{kj}), & |q_j(t)| = X_j, \\ v^{**}_{kj}, & |q_j(t)| > X_j. \end{cases}$$

Similarly , there exist $\overline{\xi}_{kj}(t) \in co(\underline{u}_{kj}, \overline{u}_{kj})$, $\overline{\zeta}_{kj}(t) \in co(\underline{v}_{kj}, \overline{v}_{kj})$, $k, j = 1, 2, \cdots, n$, such that

$$\begin{aligned} {}^cD^\eta_t q_k(t) = &- w_k q_k(t) + \sum_{j=1}^{n} \Big(\overline{\xi}_{kj}(t) + \Delta\overline{u}_{kj}(t)\Big)\phi_j(q_j(t)) + \sum_{j=1}^{n} \Big(\overline{\zeta}_{kj}(t) \\ &+ \Delta\overline{v}_{kj}(t)\Big)\varphi_j(q_j(t-\tau_j)) + I_k(t) + U_k(t),\ k = 1, 2, \cdots, n,\ t \geq 0. \end{aligned} \tag{10}$$

To establish the error system between memristive neural networks (3) and (8), the definition of the error vector is first given by

$$z(t) = q(t) - \Xi(t)p(t), \tag{11}$$

where $z(t) = (z_1(t), z_2(t), \cdots, z_n(t))^T$, $q(t) = (q_1(t), q_2(t), \cdots, q_n(t))^T$, $p(t) = (p_1(t), p_2(t), \cdots, p_n(t))^T$ and $\Xi(t) = (\Xi_{kj})_{n\times n}(t)$ $(k, j = 1, 2, \cdots, n)$ represents a variable and bounded projective matrix. Applying Caputo derivatives for component function $z_k(t) = q_k(t) - \sum_{j=1}^{n} \Xi_{kj}(t)p_j(t)$, and combining deduced networks (7) and (10), we can obtain the fractional derivative of the error function below.

$$\begin{aligned} {}^cD_t^\eta z_k(t) =& {}^cD_t^\eta q_k(t) - {}^cD_t^\eta \Big(\sum_{j=1}^{n} \Xi_{kj}(t)p_j(t) \Big) \\ =& - w_k q_k(t) + \sum_{j=1}^{n} \Big(\overline{\xi}_{kj}(t) + \Delta\overline{u}_{kj}(t) \Big) \phi_j(q_j(t)) + \sum_{j=1}^{n} \Big(\overline{\zeta}_{kj}(t) \\ & + \Delta\overline{v}_{kj}(t) \Big) \varphi_j(q_j(t-\tau_j)) + I_k(t) + U_k(t) - {}^cD_t^\eta \sum_{j=1}^{n} \Xi_{kj}(t)p_j(t). \end{aligned} \tag{12}$$

Based on the above error system, a mixed impulsive feedback controller including three items is designed as below:

$$\begin{cases} U_k(t) = U_k^O(t) + U_k^F(t) + U_k^I(t), \\ U_k^O(t) = w_k \sum\limits_{j=1}^{n} \Xi_{kj}(t)p_j(t) - \sum\limits_{j=1}^{n} \Big(\overline{\xi}_{kj}(t) + \Delta\overline{u}_{kj}(t) \Big) \phi_j\Big(\sum\limits_{i=1}^{n} \Xi_{ji}(t)p_i(t) \Big) - \sum\limits_{j=1}^{n} \Big(\overline{\zeta}_{kj}(t) \\ \qquad + \Delta\overline{v}_{kj}(t) \Big) \varphi_j\Big(\sum\limits_{i=1}^{n} \Xi_{ji}(t-\tau_i)p_i(t-\tau_i) \Big) + {}^cD_t^\eta \sum\limits_{j=1}^{n} \Xi_{kj}(t)p_j(t) - I_k(t), \\ U_k^F(t) = -d_k z_k(t) - d_k^\tau z_k(t-\tau_k), \\ U_k^I(t) = \sum\limits_{\sigma=1}^{\infty} \varpi_k z_k(t)\delta(t-t_\sigma), \end{cases} \tag{13}$$

where $d_k, d_k^\tau (k = 1, 2, \cdots, n)$ are feedback control strengths and $\varpi_k (k = 1, 2, \cdots, n)$ shows the impulsive control strength. $\delta(\cdot)$ represents the Dirac delta function. Combining error system (12) and mixed impulsive controller (13), one can obtain

$$\begin{cases} {}^cD_t^\eta z_k(t) \\ \quad = -w_k \Big(q_k(t) - \sum\limits_{j=1}^{n} \Xi_{kj}(t)p_j(t) \Big) + \sum\limits_{j=1}^{n} \Big(\overline{\xi}_{kj}(t) + \Delta\overline{u}_{kj}(t) \Big) \Big[\phi_j(q_j(t)) - \phi_j\Big(\sum\limits_{i=1}^{n} \Xi_{ji}(t)p_i(t) \Big) \Big] \\ \qquad + \sum\limits_{j=1}^{n} \Big(\overline{\zeta}_{kj}(t) + \Delta\overline{v}_{kj}(t) \Big) \Big[\varphi_j(q_j(t-\tau_j)) - \varphi_j\Big(\sum\limits_{i=1}^{n} \Xi_{ji}(t-\tau_i)p_i(t-\tau_i) \Big) \Big] \\ \qquad - d_k z_k(t) - d_k^\tau z_k(t-\tau_k), \ t \neq t_\sigma, \\ \Delta z_k(t_\sigma) = z_k(t_\sigma^+) - z_k(t_\sigma^-) = \varpi_k z_k(t_\sigma^-), \ t = t_\sigma, \end{cases} \tag{14}$$

where $z_k(t_\sigma^+) = \lim_{t\to t_\sigma^+} z_k(t)$ and $z_k(t_\sigma^-) = \lim_{t\to t_\sigma^-} z_k(t)$.

Remark 1. *The mixed control schemes in equation (13) comprise three significant parts. $U_k^O(t)$ and $U_k^F(t)$ represent the open loop and feedback controllers, while considering historical status information in time-delayed intervals. $U_k^I(t)$ denotes the impulsive sampling controller, which plays a motivating role at the impulse instants. Compared to the memoryless continuous feedback input, we comprehensively utilize the state information in the time-delayed interval and the sampling information at the impulse moments, making it easier to quickly obtain good synchronization results.*

Assumption 1. *For the nonlinear mappings ϕ_j and φ_j, there are nonnegative scalars $\tilde{\phi}_j$ and $\tilde{\varphi}_j$ satisfying*

$$|\phi_j(q) - \phi_j(p)| \leq \tilde{\phi}_j|q-p|, \quad |\varphi_j(q) - \varphi_j(p)| \leq \tilde{\varphi}_j|q-p|, \ j = 1, 2, \cdots, n, \tag{15}$$

for $\forall q, p \in R$.

Assumption 2. *All elements in projective scaling matrix $\Xi(t)$ are continuously differentiable, and each row of the matrix has at least one non-zero element.*

Definition 3. *Master system (3) and slave system (8) can accomplish the TFMPS, if the error vector conforms to $\lim_{t\to+\infty} \|z(t)\| = \lim_{t\to+\infty} \|q(t) - \Xi(t)p(t)\| = 0$.*

Remark 2. *By selecting predigested forms of projection matrix $\Xi(t)$, we can obtain different projection synchronization modes as below:*
(1) Choosing matrix $\Xi(t) = (\Xi_{kj})_{n\times n}$, the TFMPS could degenerate into the matrix PS [41].
(2) Choosing matrix $\Xi(t) = diag(C_1, C_2, \cdots, C_n)$, the TFMPS could degenerate into the modified PS [38].
(3) Choosing matrix $\Xi(t) = -I$, the TFMPS could degenerate into the anti-synchronization [42].
(4) Choosing matrix $\Xi(t) = I$, the TFMPS could degenerate into the complete synchronization [29].
The synchronization mode in this article can be seen as a generalized form of the aforementioned synchronization modes, as the elements of the projection matrix in this study can be time-varying functions rather than constants or diagonal forms.

Lemma 1 ([43])**.** *Consider a fractional multi-delayed system as below:*

$${}^{c}D_t^{\eta} Y(t) = AY(t) + \bar{A}Y(t-\tau), \ 0 < \eta < 1, \tag{16}$$

where $Y(t) = (Y_1(t), Y_2(t), \cdots, Y_n(t))^T$, $Y(t-\tau) = (Y_1(t-\tau_1), Y_2(t-\tau_2), \cdots, Y_n(t-\tau_n))^T$, $A = (a_{kj})_{n\times n}$, and $\bar{A} = (\bar{a}_{kj})_{n\times n}$. Assuming the eigenvalues of multi-delayed Equation (16) meet the constraint $|arg(\lambda)| > \frac{\pi}{2}$ and the equation $det(\Delta(s)) = 0$ does not have pure imaginary solutions for $\forall\ \tau_j > 0$, one can attain that the zero solution of (16) can be globally asymptotically stable.

Lemma 2 ([7])**.** *Suppose that $0 < \eta < 1$, $u(t) \in \mathbb{C}([t_0, +\infty), \mathbb{R})$ is differentiable. If one can find a point $t' > t_0$ satisfying $u(t') = 0$ and $u(t) < 0$ for $t_0 \leq t < t'$, then ${}^{c}D_{t'}^{\eta} u(t') > 0$.*

Lemma 3 ([44])**.** *Assume that $w(t) \in \mathbb{R}^n$ is a differentiable function, we have*

$${}^{c}D_t^{\eta} w^T(t) w(t) \leq 2w^T(t) {}^{c}D_t^{\eta} w(t), \ 0 < \eta < 1. \tag{17}$$

Lemma 4 ([45])**.** *The following matrix inequality*

$$\begin{bmatrix} \mathcal{N}_{11} & \mathcal{N}_{12} \\ \mathcal{N}_{12}^T & \mathcal{N}_{22} \end{bmatrix} < 0 \tag{18}$$

is equivalent to condition (I) *or condition* (II) *as below:*

$$\text{(I)}\ \mathcal{N}_{11} < 0, \mathcal{N}_{22} - \mathcal{N}_{12}^T \mathcal{N}_{11}^{-1} \mathcal{N}_{12} < 0;$$

$$\text{(II)}\ \mathcal{N}_{22} < 0, \mathcal{N}_{11} - \mathcal{N}_{12} \mathcal{N}_{22}^{-1} \mathcal{N}_{12}^T < 0,$$

where $\mathcal{N}_{11}^T = \mathcal{N}_{11}$ and $\mathcal{N}_{22}^T = \mathcal{N}_{22}$.

Lemma 5. *Let nonnegative functions $f(t)$ and $g(t)$ satisfying*

$$\begin{cases} {}^cD_t^\eta f(t) \le -\underline{\epsilon} f(t) + \sum\limits_{j=1}^{n} \epsilon_j(t) f(t-\tau_j(t)) + \overline{\epsilon}(t) \int_{t-\tau}^{t} f(s)ds, \ t \ne t_\sigma, \\ f(t_\sigma) \le \pi_\sigma f(t_\sigma^-), \ \sigma \in \mathbb{Z}_+, \\ f(t) = f_0(t), \ t \in [t_0-\tau, t_0], \end{cases} \tag{19}$$

and

$$\begin{cases} {}^cD_t^\eta g(t) = -\underline{\epsilon} g(t) + \sum\limits_{j=1}^{n} \epsilon_j(t) g(t-\tau_j(t)) + \overline{\epsilon}(t) \int_{t-\tau}^{t} g(s)ds, \ t \ne t_\sigma, \\ g(t) = g_0(t), \ t \in [t_0-\tau, t_0], \end{cases} \tag{20}$$

where $0 < \eta < 1, 0 < \pi_\sigma \le 1$, $\underline{\epsilon} \in \mathbb{R}$, and $0 \le \tau_j(t) \le \tau (j = 1, 2, \cdots, n)$. $\overline{\epsilon}(t)$ and $\epsilon_j(t)$ are continuous and nonnegative real-valued functions. Then $f_0(t) \le g_0(t)$ for $t_0 - \tau \le t \le t_0$ yields $f(t) \le g(t)$ for $t \ge t_0$.

Proof. Confirm this conclusion using the mathematical induction method. First, we shall validate that $f(t) \le g(t)$, $t \in [t_0, t_1)$. Evidently, $f(t) \le g(t)$ means $f(t) < \varepsilon g(t)$ if $\varepsilon > 1$ denotes any constant. Assume the result $f(t) \le g(t)$ for $t \in [t_0, t_1)$ is wrong. Considering that $f_0(t) \le g_0(t)$ for $t \in [t_0 - \tau, t_0]$ and the continuity of $f(t)$ and $g(t)$ in $[t_0, t_1)$, there exists $t' \in [t_0, t_1)$ satisfying

$$f(t) < \varepsilon g(t) \text{ for } \forall t \in [t_0 - \tau, t'), \text{ and } f(t') = \varepsilon g(t'), \tag{21}$$

where $\varepsilon > 1$ represents any constant. By utilizing Lemma 2, one can obtain

$${}^cD_{t'}^\eta f(t') > \varepsilon {}^cD_{t'}^\eta g(t'). \tag{22}$$

From another perspective, it derives from (19)–(21) that

$$\begin{aligned} &{}^cD_{t'}^\eta f(t') \\ &\le -\underline{\epsilon} f(t') + \epsilon_1(t') f(t'-\tau_1(t')) + \epsilon_2(t') f(t'-\tau_2(t')) + \cdots + \epsilon_n(t') f(t'-\tau_n(t')) \\ &\quad + \overline{\epsilon}(t') \int_{t'-\tau}^{t'} f(s)ds \\ &\le -\underline{\epsilon}\varepsilon g(t') + \epsilon_1(t')\varepsilon g(t'-\tau_1(t')) + \epsilon_2(t')\varepsilon g(t'-\tau_2(t')) + \cdots + \epsilon_n(t')\varepsilon g(t'-\tau_n(t')) \\ &\quad + \overline{\epsilon}(t')\varepsilon \int_{t'-\tau}^{t'} g(s)ds \\ &= \varepsilon \Big[-\underline{\epsilon} g(t') + \epsilon_1(t') g(t'-\tau_1(t')) + \epsilon_2(t') g(t'-\tau_2(t')) + \cdots + \epsilon_n(t') g(t'-\tau_n(t')) \\ &\quad + \overline{\epsilon}(t') \int_{t'-\tau}^{t'} g(s)ds \Big] \\ &= \varepsilon {}^cD_{t'}^\eta g(t'), \end{aligned} \tag{23}$$

which contradicts with (22). Consequently, by using the reduction to absurdity, we can acquire

$$f(t) < \varepsilon g(t), t \in [t_0, t_1). \tag{24}$$

Let $\varepsilon \to 1$, one obtains $f(t) \le g(t)$ for $t \in [t_0, t_1)$. Suppose there exists $m \in \mathbb{Z}_+$ satisfying $f(t) \le g(t)$, $t \in [t_{\sigma-1}, t_\sigma), \sigma = 2, 3, \cdots, m$, then we obtain $f(t) \le g(t)$ for $t_0 - \tau \le t < t_m$ and $f(t_m) \le \pi_m f(t_m^-) \le \pi_m g(t_m^-) \le g(t_m^-) = g(t_m)$. Note that $g(t)$ is continuous on $[t_0 - \tau, \infty)$, utilizing the analogous stages as the proof of $f(t) \le g(t)$ in $[t_0, t_1)$, we can derive $f(t) \le g(t)$ for $t \in [t_m, t_{m+1})$. Accordingly, mathematical induction indicates that the comparison principle is correct. □

Remark 3. *MNNs constructed by integer-order calculus operators have been extensively investigated and many meaningful synchronization results have been obtained in [16–21]. However, the comparison theorem and impulsive control schemes for neural networks with integer differential operators cannot be directly applied to fractional-order neural networks since fractional-order memristive systems possess special memory and hereditary properties. Therefore, synchronization of fractional-order delayed MNNs with uncertainties using impulse feedback control remains a challenging problem since the fractional-order impulse comparison theorem with delays is rare.*

Remark 4. *To overcome the influence of delays on network stability, some kinds of literature have established useful fractional-order time-delay comparison theorems for continuous systems, such as [15,23,43]. Different from these results, the fractional-order time-delay comparison theorem established in this paper considers impulse effects and time-varying coefficients. Consequently, the comparison theorem contemplated in this paper is not only applicable to continuous network models but also can be used for discontinuous impulse networks.*

3. Synchronization Analysis Results

Before giving the principal theorem and corollary in this article, we first bring in a significant matrix symbol. Denote $\Xi_n = \text{diag}\{1+\varpi_1, 1+\varpi_2, \cdots, 1+\varpi_n\}$, then the second impulsive expression in (14) can be simply rewritten as $z(t_\sigma^+) = \Xi_n z(t_\sigma^-)$ for $\sigma \in \mathbb{Z}_+$.

Theorem 1. *Under Assumptions 1–2 and mixed impulsive feedback controller (13), the global TFMPS between memristive neural networks (3) and (8) can be achieved, if there exist suitable parameters $d_k^\tau, d_k > 0, 0 < \gamma \leq 1$, and $-2 < \varpi_k < 0$, such that*

$$\text{(i)} \begin{bmatrix} -\gamma I_n & \Xi_n^T \\ \Xi_n & -I_n \end{bmatrix} \leq 0,$$

$$\text{(ii)} \sum_{j=1}^{n} \beta_j < \underline{\beta} sin\frac{\eta\pi}{2},$$

where $\underline{\beta} = \min_{1\leq k\leq n}\Big[2(w_k+d_k) - |d_k^\tau| - \sum_{j=1}^{n}\tilde{\phi}_j(u_{kj}^+ + \rho_{kj}) - \sum_{j=1}^{n}\tilde{\phi}_k(u_{jk}^+ + \rho_{jk}) - \sum_{j=1}^{n}\tilde{\varphi}_j(v_{kj}^+ + \varrho_{kj})\Big] > 0$, *and* $\beta_j = \sum_{k=1}^{n}\tilde{\varphi}_j(v_{kj}^+ + \varrho_{kj}) + |d_j^\tau|$.

Proof. Consider an auxiliary function as below:

$$V(t) = \frac{1}{2}\sum_{k=1}^{n} z_k^2(t). \tag{25}$$

When $t \in [t_{\sigma-1}, t_\sigma)$, calculating the Caputo derivative of $V(t)$ and applying Lemma 3 yields that

$$
\begin{aligned}
&{}^{c}D_{t}^{\eta}V(t)\\
&\leq \sum_{k=1}^{n} z_k(t)\,{}^{c}D_{t}^{\eta}z_k(t)\\
&= \sum_{k=1}^{n} z_k(t)\Bigg\{ -w_k\Big(q_k(t)-\sum_{j=1}^{n}\Xi_{kj}(t)p_j(t)\Big)+\sum_{j=1}^{n}\Big(\overline{\xi}_{kj}(t)+\Delta\overline{u}_{kj}(t)\Big)\Big[\phi_j(q_j(t))\\
&\quad -\phi_j\Big(\sum_{i=1}^{n}\Xi_{ji}(t)p_i(t)\Big)\Big]+\sum_{j=1}^{n}\Big(\overline{\zeta}_{kj}(t)+\Delta\overline{v}_{kj}(t)\Big)\Big[\varphi_j(q_j(t-\tau_j))\\
&\quad -\varphi_j\Big(\sum_{i=1}^{n}\Xi_{ji}(t-\tau_i)p_i(t-\tau_i)\Big)\Big]-d_k z_k(t)-d_k^{\tau}z_k(t-\tau_k)\Bigg\}\\
&\leq \sum_{k=1}^{n}\Bigg\{ -w_k z_k^2(t)+\sum_{j=1}^{n}\Big|z_k(t)\Big(\overline{\xi}_{kj}(t)+\Delta\overline{u}_{kj}(t)\Big)\Big[\phi_j(q_j(t))-\phi_j\Big(\sum_{i=1}^{n}\Xi_{ji}(t)p_i(t)\Big)\Big]\Big|\\
&\quad +\sum_{j=1}^{n}\Big|z_k(t)\Big(\overline{\zeta}_{kj}(t)+\Delta\overline{v}_{kj}(t)\Big)\Big[\varphi_j(q_j(t-\tau_j))-\varphi_j\Big(\sum_{i=1}^{n}\Xi_{ji}(t-\tau_i)p_i(t-\tau_i)\Big)\Big]\Big|\\
&\quad -d_k z_k^2(t)+\Big|z_k(t)d_k^{\tau}z_k(t-\tau_k)\Big|\Bigg\}. \qquad (26)
\end{aligned}
$$

According to Assumption 1, one can obtain

$$
\begin{aligned}
\Big|\phi_j(q_j(t))-\phi_j\Big(\sum_{i=1}^{n}\Xi_{ji}(t)p_i(t)\Big)\Big| &\leq \tilde{\phi}_j\Big|q_j(t)-\sum_{i=1}^{n}\Xi_{ji}(t)p_i(t)\Big|\\
&= \tilde{\phi}_j|z_j(t)|, \qquad (27)
\end{aligned}
$$

$$
\begin{aligned}
\Big|\varphi_j(q_j(t-\tau_j))-\varphi_j\Big(\sum_{i=1}^{n}\Xi_{ji}(t-\tau_i)p_i(t-\tau_i)\Big)\Big| &\leq \tilde{\varphi}_j\Big|q_j(t-\tau_j)-\sum_{i=1}^{n}\Xi_{ji}(t-\tau_i)p_i(t-\tau_i)\Big|\\
&= \tilde{\varphi}_j|z_j(t-\tau_j)|. \qquad (28)
\end{aligned}
$$

From (27), we can obtain

$$
\begin{aligned}
&\Big|z_k(t)\Big(\overline{\xi}_{kj}(t)+\Delta\overline{u}_{kj}(t)\Big)\Big[\phi_j(q_j(t))-\phi_j\Big(\sum_{i=1}^{n}\Xi_{ji}(t)p_i(t)\Big)\Big]\Big|\\
&\quad \leq \tilde{\phi}_j\Big|z_k(t)\Big(\overline{\xi}_{kj}(t)+\Delta\overline{u}_{kj}(t)\Big)z_j(t)\Big|\\
&\quad \leq \frac{\tilde{\phi}_j(u_{kj}^{+}+\rho_{kj})}{2}\big(z_k^2(t)+z_j^2(t)\big). \qquad (29)
\end{aligned}
$$

From (28), we can obtain

$$
\begin{aligned}
&\Big|z_k(t)\Big(\overline{\zeta}_{kj}(t)+\Delta\overline{v}_{kj}(t)\Big)\Big[\varphi_j(q_j(t-\tau_j))-\varphi_j\Big(\sum_{i=1}^{n}\Xi_{ji}(t-\tau_i)p_i(t-\tau_i)\Big)\Big]\Big|\\
&\quad \leq \tilde{\varphi}_j\Big|z_k(t)\Big(\overline{\zeta}_{kj}(t)+\Delta\overline{v}_{kj}(t)\Big)z_j(t-\tau_j)\Big|\\
&\quad \leq \frac{\tilde{\varphi}_j(v_{kj}^{+}+\varrho_{kj})}{2}\big(z_k^2(t)+z_j^2(t-\tau_j)\big). \qquad (30)
\end{aligned}
$$

Utilizing the inequality $2x^Ty \leq x^Tx + y^Ty$, one can obtain

$$\left|z_k(t)d_k^\tau z_k(t-\tau_k)\right| \leq \frac{|d_k^\tau|}{2}\left(z_k^2(t) + z_k^2(t-\tau_k)\right). \tag{31}$$

Substituting inequalities (29)–(31) into (26), we have

$$\begin{aligned}
{}^cD_t^\eta V(t) \leq & \sum_{k=1}^{n}\Bigg[-w_k z_k^2(t) + \sum_{j=1}^{n}\frac{\tilde{\phi}_j(u_{kj}^+ + \rho_{kj})}{2}\left(z_k^2(t) + z_j^2(t)\right) + \sum_{j=1}^{n}\frac{\tilde{\varphi}_j(v_{kj}^+ + \varrho_{kj})}{2}\left(z_k^2(t)\right. \\
& \left. + z_j^2(t-\tau_j)\right) + \frac{|d_k^\tau|}{2}\left(z_k^2(t) + z_k^2(t-\tau_k)\right) - d_k z_k^2(t)\Bigg] \\
= & \sum_{k=1}^{n}\Bigg[-\Bigg(w_k + d_k - \frac{|d_k^\tau|}{2} - \sum_{j=1}^{n}\frac{\tilde{\phi}_j(u_{kj}^+ + \rho_{kj})}{2} - \sum_{j=1}^{n}\frac{\tilde{\phi}_k(u_{jk}^+ + \rho_{jk})}{2} \\
& - \sum_{j=1}^{n}\frac{\tilde{\varphi}_j(v_{kj}^+ + \varrho_{kj})}{2}\Bigg)z_k^2(t) + \sum_{j=1}^{n}\frac{\tilde{\varphi}_j(v_{kj}^+ + \varrho_{kj})}{2}z_j^2(t-\tau_j) + \frac{|d_k^\tau|}{2}z_k^2(t-\tau_k)\Bigg].
\end{aligned} \tag{32}$$

Note that $\frac{1}{2}z_j^2(t-\tau_j) \leq \frac{1}{2}(z_1(t-\tau_j), z_2(t-\tau_j), \cdots, z_n(t-\tau_j))(z_1(t-\tau_j), z_2(t-\tau_j), \cdots, z_n(t-\tau_j))^T = V(t-\tau_j)$.

Take $\beta_j = \sum\limits_{k=1}^{n}\tilde{\varphi}_j(v_{kj}^+ + \varrho_{kj}) + |d_j^\tau|$, then one can obtain

$$\begin{aligned}
{}^cD_t^\eta V(t) \leq & -\min_{1\leq k\leq n}\Bigg(2(w_k + d_k) - |d_k^\tau| - \sum_{j=1}^{n}\tilde{\phi}_j(u_{kj}^+ + \rho_{kj}) - \sum_{j=1}^{n}\tilde{\phi}_k(u_{jk}^+ + \rho_{jk}) \\
& - \sum_{j=1}^{n}\tilde{\varphi}_j(v_{kj}^+ + \varrho_{kj})\Bigg)V(t) + \sum_{j=1}^{n}\Bigg(\sum_{k=1}^{n}\tilde{\varphi}_j(v_{kj}^+ + \varrho_{kj}) + |d_j^\tau|\Bigg)V(t-\tau_j) \\
= & -\underline{\beta}V(t) + \sum_{j=1}^{n}\beta_j V(t-\tau_j),
\end{aligned} \tag{33}$$

where

$$\begin{aligned}
\underline{\beta} &= \min_{1\leq k\leq n}\left[2(w_k + d_k) - |d_k^\tau| - \sum_{j=1}^{n}\tilde{\phi}_j(u_{kj}^+ + \rho_{kj}) - \sum_{j=1}^{n}\tilde{\phi}_k(u_{jk}^+ + \rho_{jk}) - \sum_{j=1}^{n}\tilde{\varphi}_j(v_{kj}^+ + \varrho_{kj})\right], \\
\beta_j &= \sum_{k=1}^{n}\tilde{\varphi}_j(v_{kj}^+ + \varrho_{kj}) + |d_j^\tau|.
\end{aligned}$$

Based on condition (i) of Theorem 1, we have

$$\begin{bmatrix} -\gamma z^T(t_\sigma^-)z(t_\sigma^-) & z^T(t_\sigma^-)\Xi_n^T \\ \Xi_n z(t_\sigma^-) & -I_n \end{bmatrix} = \begin{bmatrix} z^T(t_\sigma^-) & 0 \\ 0 & I_n \end{bmatrix}\begin{bmatrix} -\gamma I_n & \Xi_n^T \\ \Xi_n & -I_n \end{bmatrix}\begin{bmatrix} z(t_\sigma^-) & 0 \\ 0 & I_n \end{bmatrix} \leq 0. \tag{34}$$

It follows from Lemma 4 and inequality (33) that

$$-\gamma z^T(t_\sigma^-)z(t_\sigma^-) + z^T(t_\sigma^-)\Xi_n^T\Xi_n z(t_\sigma^-) \leq 0. \tag{35}$$

Combining the mathematical expression of $V(t)$ and inequality (34), when $t = t_\sigma$, we have

$$V(t_\sigma^+) = \frac{1}{2}z^T(t_\sigma^+)z(t_\sigma^+) = \frac{1}{2}z^T(t_\sigma^-)\Xi_n^T\Xi_n z(t_\sigma^-) \leq \gamma V(t_\sigma^-), \tag{36}$$

where $0 < \gamma \leq 1$. From inequalities (33) and (36), one has

$$\begin{cases} {}^cD_t^\eta V(t) \leq -\underline{\beta}V(t) + \sum\limits_{j=1}^{n} \beta_j V(t-\tau_j),\ t \in [t_{\sigma-1}, t_\sigma), \\ V(t_\sigma^+) \leq \gamma V(t_\sigma^-),\ \sigma \in Z_+. \end{cases} \tag{37}$$

Contemplate a Caputo fractional-order differential system as below:

$${}^cD_t^\eta \mu(t) = -\underline{\beta}\mu(t) + \sum_{j=1}^{n} \beta_j \mu(t-\tau_j), \tag{38}$$

where $\mu(t)$ is continuous in the interval $[t_0 - \tau, \infty)$ and it owns identical starting values with $V(t)$. Taking into consideration the condition $0 < \gamma \leq 1$ and utilizing Lemma 5, we acquire

$$0 \leq V(t) \leq \mu(t). \tag{39}$$

Applying the Laplace transform tool for differential system (38) gives that

$$\begin{aligned} s^\eta \mu(s) - s^{\eta-1}\mu(t_0) &= -\underline{\beta}\mu(s) + \sum_{j=1}^{n} \beta_j \int_{t_0}^{+\infty} e^{-st}\mu(t-\tau_j)dt \\ &= -\underline{\beta}\mu(s) + \sum_{j=1}^{n} \beta_j \int_{t_0-\tau_j}^{+\infty} e^{-s(t+\tau_j)}\mu(t)dt \\ &= -\underline{\beta}\mu(s) + \sum_{j=1}^{n} \beta_j e^{-s\tau_j}\Big(\int_{t_0-\tau_j}^{t_0} e^{-st}\mu(t)dt + \int_{t_0}^{+\infty} e^{-st}\mu(t)dt\Big) \\ &= -\underline{\beta}\mu(s) + \sum_{j=1}^{n} \beta_j e^{-s\tau_j}\mu(s) + \sum_{j=1}^{n} \beta_j e^{-s\tau_j}\int_{t_0-\tau_j}^{t_0} e^{-st}\mu(t)dt. \end{aligned} \tag{40}$$

Combining transformed expression (40) and Lemma 1, we can derive

$$\det(\Delta(s))\mu(s) = s^{\eta-1}\mu(t_0) + \sum_{j=1}^{n} \beta_j e^{-s\tau_j}\int_{t_0-\tau_j}^{t_0} e^{-st}\mu(t)dt, \tag{41}$$

where characteristic polynomial $\det(\Delta(s)) = s^\eta + \underline{\beta} - \sum\limits_{j=1}^{n} \beta_j e^{-s\tau_j}$. Next, contemplate the approach of the proof by contradiction to illustrate that the equation $\det(\Delta(s)) = 0$ has no pure imaginary solutions. Suppose a pure imaginary number $s = \Re i = |\Re|(\cos\frac{\pi}{2} + i\sin(\pm\frac{\pi}{2}))$, where $\Re \in \mathbb{R}$. If $\Re > 0$, choose $i\sin(\frac{\pi}{2})$; otherwise, choose $i\sin(-\frac{\pi}{2})$. Substituting $s = \Re i = |\Re|(\cos\frac{\pi}{2} + i\sin(\pm\frac{\pi}{2}))$ into $\det(\Delta(s)) = 0$ and utilizing the well-known Euler formula, we can obtain

$$|\Re|^\eta\Big(\cos\frac{\eta\pi}{2} + i\sin(\frac{\pm\eta\pi}{2})\Big) + \underline{\beta} - \sum_{j=1}^{n} \beta_j(\cos\Re\tau_j - i\sin\Re\tau_j) = 0. \tag{42}$$

Note that the equal of two complex numbers is equivalent to the corresponding equal of the real part and imaginary part separately. Separating real and imaginary parts in (42) gives

$$\begin{cases} |\Re|^{\eta}\cos\frac{\eta\pi}{2} + \underline{\beta} = \sum\limits_{j=1}^{n} \beta_j \cos\Re\tau_j, \\ |\Re|^{\eta}\sin\frac{(\pm\eta\pi)}{2} = \sum\limits_{j=1}^{n} \beta_j \sin\Re\tau_j. \end{cases} \tag{43}$$

Squaring the above two equations first and then adding them together yields

$$|\Re|^{2\eta} + 2\underline{\beta}\cos\frac{\eta\pi}{2}|\Re|^{\eta} + \underline{\beta}^2 = \Big(\sum_{j=1}^{n} \beta_j \cos\Re\tau_j\Big)^2 + \Big(\sum_{j=1}^{n} \beta_j \sin\Re\tau_j\Big)^2. \tag{44}$$

Note the following trigonometric equality

$$\begin{aligned} \Big(\sum_{j=1}^{n} \beta_j \cos\Re\tau_j\Big)^2 + \Big(\sum_{j=1}^{n} \beta_j \sin\Re\tau_j\Big)^2 &= \sum_{i=1}^{n}\sum_{j=1}^{n} \beta_i\beta_j \cos\Re\tau_j\cos\Re\tau_j + \sum_{i=1}^{n}\sum_{j=1}^{n} \beta_i\beta_j \sin\Re\tau_j\sin\Re\tau_j \\ &= \sum_{i=1}^{n}\sum_{j=1}^{n} \beta_i\beta_j \cos\Re(\tau_i - \tau_j). \end{aligned} \tag{45}$$

Substituting equation (45) into equation (44), we have

$$|\Re|^{2\eta} + 2\underline{\beta}\cos\frac{\eta\pi}{2}|\Re|^{\eta} + \underline{\beta}^2 = \sum_{i=1}^{n}\sum_{j=1}^{n} \beta_i\beta_j \cos\Re(\tau_i - \tau_j). \tag{46}$$

Considering a two-order polynomial function $\mathcal{L}(x) = x^2 + 2\underline{\beta}\cos\frac{\eta\pi}{2}x + \underline{\beta}^2 - \sum\limits_{i=1}^{n}\sum\limits_{j=1}^{n} \beta_i\beta_j\cos\Re(\tau_i - \tau_j)$. One can obtain $\mathcal{L}(0) = \underline{\beta}^2 - \sum\limits_{i=1}^{n}\sum\limits_{j=1}^{n} \beta_i\beta_j\cos\Re(\tau_i - \tau_j) > 0$, since $\sum\limits_{j=1}^{n} \beta_j < \underline{\beta}\sin\frac{\eta\pi}{2}$, $0 < \eta < 1$, $\beta_j > 0 (j = 1, 2, \cdots, n)$. Moreover, $\mathcal{L}(x)$ represents a two-order polynomial function with a strictly monotonically increasing interval $[-\underline{\beta}\cos\frac{\eta\pi}{2}, +\infty)$, we can obtain $\mathcal{L}(|\Re|^{\eta}) > \mathcal{L}(0) > 0$. Hence, $|\Re|^{2\eta} + 2\underline{\beta}\cos\frac{\eta\pi}{2}|\Re|^{\eta} + \underline{\beta}^2 - \sum\limits_{i=1}^{n}\sum\limits_{j=1}^{n} \beta_i\beta_j\cos\Re(\tau_i - \tau_j) > 0$, which shows equation (46) has no solution, namely, we cannot find a pure imaginary solution that meets the mathematical Equation $\det(\Delta(s)) = 0$. In addition, when $\sum\limits_{j=1}^{n} \beta_j < \underline{\beta}\sin\frac{\eta\pi}{2}$, one can gain $|arg(-\underline{\beta} + \sum\limits_{j=1}^{n} \beta_j)| > \frac{\pi}{2}$. Based on Lemma 1, the zero solution of system (38) is asymptotically stable and $\lim_{t\to+\infty} \mu(t) = 0$. According to inequality (39) and the Sandwich theorem, one can derive that $\lim_{t\to+\infty} V(t) = 0$, and the time-varying function matrix projection synchronization of memristive systems can be achieved. □

Remark 5. *The feedback control part mainly utilizes the current error information $z_k(t)$ and assists the delayed error information $z_k(t - \tau_k)$ as a supplement. To accelerate the synchronization efficiency of the driver network and the response network, selecting the relatively large adjustable parameter d_k and the relatively small parameter d_k^{τ} can ensure that the condition $\underline{\beta} = \min_{1\le k\le n}\Big[2(w_k + d_k) - |d_k^{\tau}| - \sum\limits_{j=1}^{n} \tilde{\phi}_j(u_{kj}^{+} + \rho_{kj}) - \sum\limits_{j=1}^{n} \tilde{\phi}_k(u_{jk}^{+} + \rho_{jk}) - \sum\limits_{j=1}^{n} \tilde{\varphi}_j(v_{kj}^{+} + \varrho_{kj})\Big] > 0$ in Theorem 1 is more easily met. To minimize control costs, we generally choose the minimum d_k that satisfies condition (ii).*

Remark 6. *Different from continuous feedback control, mixed impulse feedback control considered in this paper is a discontinuous control strategy with the merit of high transmission security. If we replace the mixed impulse control with pure impulse control, the parameter $\underline{\beta}$ in condition (ii) of*

Theorem 1 may become negative. Since $\beta_j (j = 1, 2, \cdots, m)$ is positive, this will make condition (ii) not hold. Accordingly, the feedback parts of our controller are indispensable.

Remark 7. *The impulsive control part $U_k^I(t)$ and condition (i) in Theorem 1 ensure that condition $V(t_\sigma^+) \leq \gamma V(t_\sigma^-)$ in (37) is satisfied. This lays the important foundation for utilizing the proposed comparison theorem and Laplace transforms to complete the stability analysis of error systems.*

Especially, with time-varying uncertainties $\Delta\overline{u}_{kj}(t) = 0$ and $\Delta\overline{v}_{kj}(t) = 0$, memristive neural networks (3) with the Caputo derivative can be simplified as

$$\begin{aligned} {}^cD_t^\eta p_k(t) = & -w_k p_k(t) + \sum_{j=1}^{n} u_{kj}(p_j(t))\phi_j(p_j(t)) + \sum_{j=1}^{n} v_{kj}(p_j(t))\varphi_j(p_j(t-\tau_j)) \\ & + I_k(t),\ k = 1, 2, \cdots, n,\ t \geq 0. \end{aligned} \tag{47}$$

Correspondingly, response memristive neural networks are simplified by

$$\begin{aligned} {}^cD_t^\eta q_k(t) = & -w_k q_k(t) + \sum_{j=1}^{n} u_{kj}(q_j(t))\phi_j(q_j(t)) + \sum_{j=1}^{n} v_{kj}(q_j(t))\varphi_j(q_j(t-\tau_j)) \\ & + I_k(t) + U_k(t),\ k = 1, 2, \cdots, n,\ t \geq 0. \end{aligned} \tag{48}$$

Construct the external control input $U_k(t)$ as

$$\begin{cases} U_k(t) = U_k^O(t) + U_k^F(t) + U_k^I(t), \\ U_k^O(t) = w_k \sum\limits_{j=1}^{n} \Xi_{kj}(t) p_j(t) - \sum\limits_{j=1}^{n} \overline{\xi}_{kj}(t)\phi_j\Big(\sum\limits_{i=1}^{n} \Xi_{ji}(t) p_i(t)\Big) \\ \qquad - \sum\limits_{j=1}^{n} \overline{\zeta}_{kj}(t)\varphi_j\Big(\sum\limits_{i=1}^{n} \Xi_{ji}(t-\tau_i) p_i(t-\tau_i)\Big) + {}^cD_t^\eta \sum\limits_{j=1}^{n} \Xi_{kj}(t) p_j(t) - I_k(t), \\ U_k^F(t) = -d_k z_k(t) - d_k^\tau z_k(t-\tau_k), \\ U_k^I(t) = \sum\limits_{\sigma=1}^{\infty} \omega_k z_k(t)\delta(t - t_\sigma). \end{cases} \tag{49}$$

Employing the similar proof approach in Theorem 1, one can acquire the following Corollary.

Corollary 1. *Under Assumptions 1 and 2 and mixed impulsive feedback controller (49), the global TFMPS between memristive neural networks (47) and (48) can be achieved, if there exist suitable parameters $d_k^\tau, d_k > 0, 0 < \gamma \leq 1$ and $-2 < \omega_k < 0$, such that*

$$\text{(i)} \begin{bmatrix} -\gamma I_n & \Xi_n^T \\ \Xi_n & -I_n \end{bmatrix} \leq 0,$$

$$\text{(ii)} \sum_{j=1}^{n} \beta_j < \underline{\beta} sin\frac{\eta\pi}{2},$$

where $\underline{\beta} = \min_{1\leq k\leq n}\left[2(w_k + d_k) - |d_k^\tau| - \sum\limits_{j=1}^{n} \tilde{\phi}_j u_{kj}^+ - \sum\limits_{j=1}^{n} \tilde{\phi}_k u_{jk}^+ - \sum\limits_{j=1}^{n} \tilde{\varphi}_j v_{kj}^+\right] > 0$, *and* $\beta_j = \sum\limits_{k=1}^{n} \tilde{\varphi}_j v_{kj}^+ + |d_j^\tau|$.

Remark 8. *Based on the system environment and control requirements, when the impulsive strength satisfies $-2 < \omega_k < 0$ and $\sum_{j=1}^{n} \beta_j < \underline{\beta} sin\frac{\eta\pi}{2}$, impulsive intervals $t_k - t_{k-1}$ are not tightly constrained by time delays.*

4. Illustrative Experiments

In this section, we will present simulation experiments with different dimensions to verify the applicability of Theorem 1.

Example 1. *Take the following two-dimensional fractional-order delayed memristive networks with bounded uncertainties as the drive system.*

$$\begin{cases} {}^{c}D_t^{\eta} p_1(t) = -w_1 p_1(t) + \sum\limits_{j=1}^{2} \left(u_{1j}(p_j) + \Delta\overline{u}_{1j}\right) tanh(p_j(t)) + \sum\limits_{j=1}^{2} \left(v_{1j}(p_j) + \Delta\overline{v}_{1j}\right) \\ \qquad \times tanh(p_j(t-\tau_j)) + I_1(t), \\ {}^{c}D_t^{\eta} p_2(t) = -w_2 p_2(t) + \sum\limits_{j=1}^{2} \left(u_{2j}(p_j) + \Delta\overline{u}_{2j}\right) tanh(p_j(t)) + \sum\limits_{j=1}^{2} \left(v_{2j}(p_j) + \Delta\overline{v}_{2j}\right) \\ \qquad \times tanh(p_j(t-\tau_j)) + I_2(t), \end{cases} \tag{50}$$

where

$$u_{11}(p_1) = \begin{cases} 2.25, & |p_1(t)| < 1, \\ 2.15, & |p_1(t)| > 1, \end{cases} \quad u_{12}(p_2) = \begin{cases} -2.15, & |p_2(t)| < 1, \\ -2.25, & |p_2(t)| > 1, \end{cases}$$

$$u_{21}(p_1) = \begin{cases} -0.45, & |p_1(t)| < 1, \\ -0.4, & |p_1(t)| > 1, \end{cases} \quad u_{22}(p_2) = \begin{cases} 2.65, & |p_2(t)| < 1, \\ 2.7, & |p_2(t)| > 1, \end{cases}$$

$$v_{11}(p_1) = \begin{cases} -3.85, & |p_1(t)| < 1, \\ -3.75, & |p_1(t)| > 1, \end{cases} \quad v_{12}(p_2) = \begin{cases} -2.5, & |p_2(t)| < 1, \\ -2.6, & |p_2(t)| > 1, \end{cases}$$

$$v_{21}(p_1) = \begin{cases} -1.85, & |p_1(t)| < 1, \\ -1.75, & |p_1(t)| > 1, \end{cases} \quad v_{22}(p_2) = \begin{cases} -3.65, & |p_2(t)| < 1, \\ -3.55, & |p_2(t)| > 1, \end{cases}$$

$\eta = 0.98$, $\tau_1 = 0.1$, $\tau_2 = 0.2$, $w_1 = 2.5$, $w_2 = 1.5$, $I_1(t) = -0.1\ sint$, $I_2(t) = 0.02\ cost$, $\Delta\overline{u}_{kj} = \begin{bmatrix} 0.3\ sint & 0.2\ cost \\ 0.2\ sint & 0.1\ cost \end{bmatrix}$ *and* $\Delta\overline{v}_{kj} = \begin{bmatrix} -0.6\ cost & 0.2\ sint \\ 0.1\ cost & -0.1\ sint \end{bmatrix}$.

According to drive neural networks (50), the response neural networks can be given as

$$\begin{cases} {}^{c}D_t^{\eta} q_1(t) = -w_1 q_1(t) + \sum\limits_{j=1}^{2} \left(u_{1j}(q_j) + \Delta\overline{u}_{1j}\right) \tanh(q_j(t)) + \sum\limits_{j=1}^{2} \left(v_{1j}(q_j) + \Delta\overline{v}_{1j}\right) \\ \qquad \times \tanh(q_j(t-\tau_j)) + I_1(t) + U_1(t), \\ {}^{c}D_t^{\eta} q_2(t) = -w_2 q_2(t) + \sum\limits_{j=1}^{2} \left(u_{2j}(q_j) + \Delta\overline{u}_{2j}\right) \tanh(q_j(t)) + \sum\limits_{j=1}^{2} \left(v_{2j}(q_j) + \Delta\overline{v}_{2j}\right) \\ \qquad \times \tanh(q_j(t-\tau_j)) + I_2(t) + U_2(t), \end{cases} \tag{51}$$

where

$$u_{11}(q_1) = \begin{cases} 2.25, & |q_1(t)| < 1, \\ 2.15, & |q_1(t)| > 1, \end{cases} \quad u_{12}(q_2) = \begin{cases} -2.15, & |q_2(t)| < 1, \\ -2.25, & |q_2(t)| > 1, \end{cases}$$

$$u_{21}(q_1) = \begin{cases} -0.45, & |q_1(t)| < 1, \\ -0.4, & |q_1(t)| > 1, \end{cases} \quad u_{22}(q_2) = \begin{cases} 2.65, & |q_2(t)| < 1, \\ 2.7, & |q_2(t)| > 1, \end{cases}$$

$$v_{11}(q_1) = \begin{cases} -3.85, & |q_1(t)| < 1, \\ -3.75, & |q_1(t)| > 1, \end{cases} \quad v_{12}(q_2) = \begin{cases} -2.5, & |q_2(t)| < 1, \\ -2.6, & |q_2(t)| > 1, \end{cases}$$

$$v_{21}(q_1) = \begin{cases} -1.85, & |q_1(t)| < 1, \\ -1.75, & |q_1(t)| > 1, \end{cases} \quad v_{22}(q_2) = \begin{cases} -3.65, & |q_2(t)| < 1, \\ -3.55, & |q_2(t)| > 1, \end{cases}$$

and other network parameters have the same values as system (50). Based on the synchronization Definition and Assumption 2, choosing the time-varying projective scaling matrix as $\Xi(t) = \begin{bmatrix} 1 - \sin t & 0.4\sin t \\ -\cos t & -1.1\sin t \end{bmatrix}$, then one can obtain the error functions of TFMPS as $z_1 = q_1 - [p_1(1 - \sin t) + 0.4p_2 \sin t]$ and $z_2 = q_2 - [-p_1 \cos t - 1.1p_2 \sin t]$.

To achieve the TFMPS between Caputo FOUMNNs (50) and (51), feedback control strengths d_k and d_k^τ in (13) can be selected as $d_1 = d_2 = 15$, $d_1^\tau = d_2^\tau = 1$. The impulsive control strength and impulsive intervals can be chosen as $\varpi_k = -0.2$ and $t_\sigma - t_{\sigma-1} = 0.1$, respectively. The Lipschitz constants are set as $\tilde{\phi}_j = \tilde{\varphi}_j = 1, j = 1, 2.$, which shows that Assumption 1 is valid. Let parameter $\gamma = 0.78$, and then simple calculation shows that $\beta_1 = \sum_{k=1}^{2} \tilde{\varphi}_1(v_{k1}^+ + \varrho_{k1}) + |d_1^\tau| = 7.4$, $\beta_2 = \sum_{k=1}^{2} \tilde{\varphi}_2(v_{k2}^+ + \varrho_{k2}) + |d_2^\tau| = 7.55$, $\underline{\beta} = \min_{1 \le k \le n} \left[2(w_k + d_k) - |d_k^\tau| - \sum_{j=1}^{2} \tilde{\phi}_j(u_{kj}^+ + \rho_{kj}) - \sum_{j=1}^{2} \tilde{\phi}_k(u_{jk}^+ + \rho_{jk}) - \sum_{j=1}^{2} \tilde{\varphi}_j(v_{kj}^+ + \varrho_{kj}) \right] = 17.6$, $\sum_{j=1}^{2} \beta_j - \underline{\beta} \sin \frac{\eta\pi}{2} = -2.6412 < 0$, and $\begin{bmatrix} -0.78 I_2 & \Xi_2^T \\ \Xi_2 & -I_2 \end{bmatrix} \le 0$. Thereupon, the calculation results indicate that all parameters above meet the conditions of Theorem 1.

The initial values of memristive network systems (50) and (51) are generated randomly in the interval $[0, 1]$. By utilizing prediction-correction methods with Matlab software, the state trajectories and error functions for (50) and (51) are displayed in Figure 1. As one can see in Figure 1a,b, under the influence of scale factors, the red and blue curves in the controlled drive-response networks gradually overlap. Moreover, as shown in Figure 1c,d, the two error curves of different dimensions gradually approach zero, indicating the effectiveness of the control scheme utilized in this study. To further observe the effect of the feedback control intensity d_k on the synchronization speed, we enhance the control intensity as $d_k = 20$ and keep the remaining control intensities unchanged. Comparing Figures 1 and 2, one can easily observe that a larger non-delay feedback control intensity d_k can improve synchronization speed. Therefore, for the synchronization speed requirements of actual systems, we can flexibly choose the control intensity.

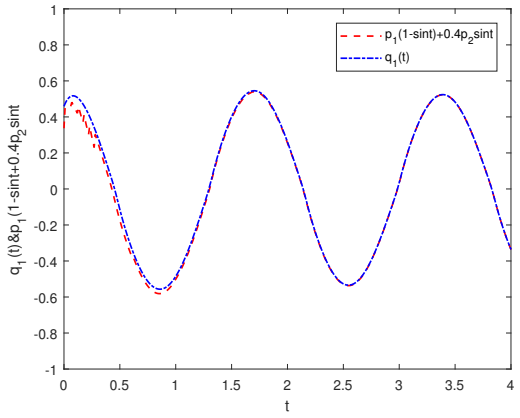

(**a**)

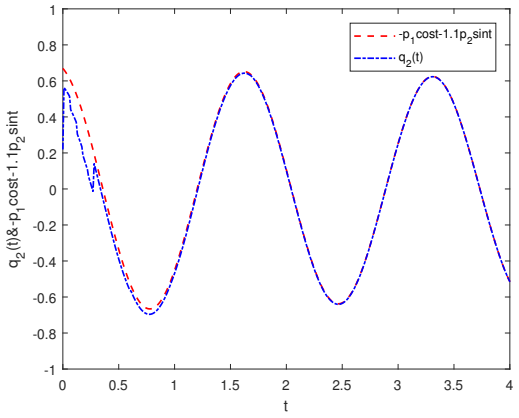

(**b**)

Figure 1. *Cont.*

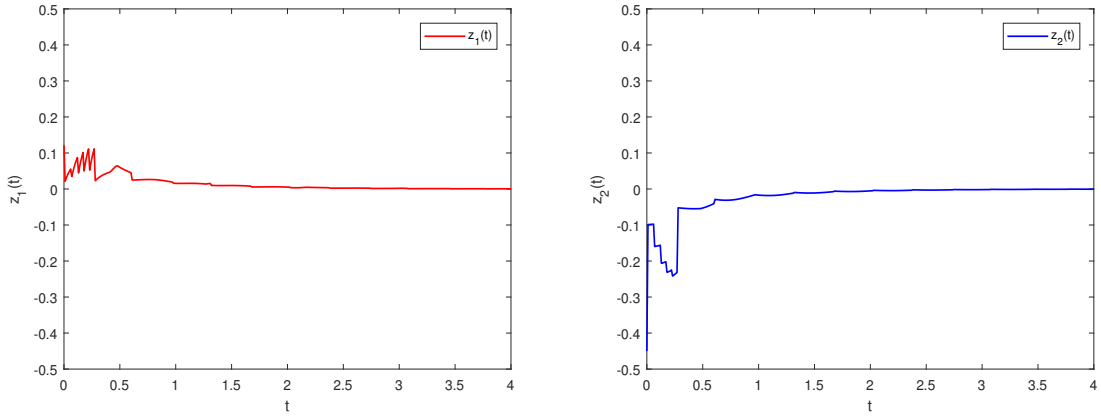

(**c**) (**d**)

Figure 1. The state trajectories and error functions in FOUMNNs (50) and (51) with control intensities $d_k = 15$ in Example 1. (**a**) $q_1(t)\&[p_1(1-\sin t)+0.4p_2\sin t]$; (**b**) $q_2(t)\&[-p_1\cos t-1.1p_2\sin t]$; (**c**) $z_1(t)$; (**d**) $z_2(t)$.

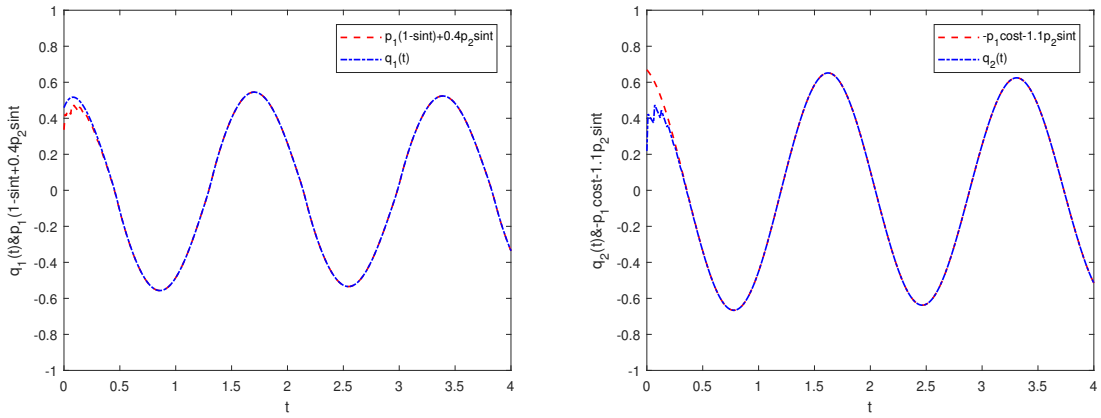

(**a**) (**b**)

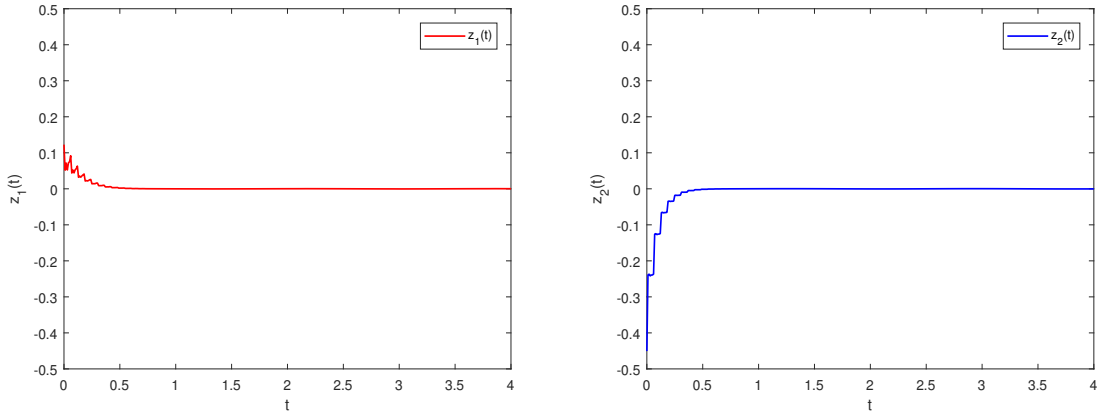

(**c**) (**d**)

Figure 2. The state trajectories and error functions in FOUMNNs (50) and (51) with control intensities $d_k = 20$ in Example 1. (**a**) $q_1(t)\&p_1(1-\sin t)+0.4p_2\sin t$; (**b**) $q_2(t)\&-p_1\cos t-1.1p_2\sin t$; (**c**) $z_1(t)$; (**d**) $z_2(t)$.

Remark 9. *Considering that the fractional-order system in this article has multiple time delays, a modified prediction-correction algorithm called Adams–Bashforth–Moulton [46] is used to solve the fractional-order equations in numerical simulations based on the Matlab software. The algorithm consists of two main steps: Adams-Bashforth prediction and Adams-Moulton correction. The product trapezoidal product rule is applied to the corrector part and the product rectangular rule is used to assess the predictor part. Therefore, the whole numerical method is easily implemented by applying these two rules, and detailed algorithm steps can be seen in [46].*

Example 2. *As the drive system, a three-dimensional fractional-order delayed memristive network with uncertainties is denoted as*

$$\begin{cases} {}^{c}D_t^{\eta} p_1(t) = -w_1 p_1(t) + \sum\limits_{j=1}^{3} \left(u_{1j}(p_j) + \Delta\overline{u}_{1j}\right) tanh(p_j(t)) + \sum\limits_{j=1}^{3} \left(v_{1j}(p_j) + \Delta\overline{v}_{1j}\right) \\ \qquad \times tanh(p_j(t-\tau_j)) + I_1(t), \\ {}^{c}D_t^{\eta} p_2(t) = -w_2 p_2(t) + \sum\limits_{j=1}^{3} \left(u_{2j}(p_j) + \Delta\overline{u}_{2j}\right) tanh(p_j(t)) + \sum\limits_{j=1}^{3} \left(v_{2j}(p_j) + \Delta\overline{v}_{2j}\right) \\ \qquad \times tanh(p_j(t-\tau_j)) + I_2(t), \\ {}^{c}D_t^{\eta} p_3(t) = -w_3 p_3(t) + \sum\limits_{j=1}^{3} \left(u_{3j}(p_j) + \Delta\overline{u}_{3j}\right) tanh(p_j(t)) + \sum\limits_{j=1}^{3} \left(v_{3j}(p_j) + \Delta\overline{v}_{3j}\right) \\ \qquad \times tanh(p_j(t-\tau_j)) + I_3(t), \end{cases} \tag{52}$$

where

$$u_{11}(p_1) = \begin{cases} 3.2, & |p_1(t)| < 1, \\ 3.1, & |p_1(t)| > 1, \end{cases} \quad u_{12}(p_2) = \begin{cases} -2.0, & |p_2(t)| < 1, \\ -1.1, & |p_2(t)| > 1, \end{cases}$$

$$u_{13}(p_3) = \begin{cases} -3.1, & |p_3(t)| < 1, \\ -4.1, & |p_3(t)| > 1, \end{cases} \quad u_{21}(p_1) = \begin{cases} 1, & |p_1(t)| < 1, \\ 0.9, & |p_1(t)| > 1, \end{cases}$$

$$u_{22}(p_2) = \begin{cases} 2.0, & |p_2(t)| < 1, \\ 1.9 + \frac{\pi}{4}, & |p_2(t)| > 1, \end{cases} \quad u_{23}(p_3) = \begin{cases} -0.9, & |p_3(t)| < 1, \\ -5, & |p_3(t)| > 1, \end{cases}$$

$$u_{31}(p_1) = \begin{cases} 3.5, & |p_1(t)| < 1, \\ 6.1, & |p_1(t)| > 1, \end{cases} \quad u_{32}(p_2) = \begin{cases} -1.2, & |p_2(t)| < 1, \\ -1.6, & |p_2(t)| > 1, \end{cases}$$

$$u_{33}(p_3) = \begin{cases} -2, & |p_3(t)| < 1, \\ -1.1, & |p_3(t)| > 1, \end{cases} \quad v_{11}(p_1) = \begin{cases} -2.2, & |p_1(t)| < 1, \\ -2.2, & |p_1(t)| > 1, \end{cases}$$

$$v_{12}(p_2) = \begin{cases} 0.15, & |p_2(t)| < 1, \\ 0.23, & |p_2(t)| > 1, \end{cases} \quad v_{13}(p_3) = \begin{cases} -0.85, & |p_3(t)| < 1, \\ 0.9, & |p_3(t)| > 1, \end{cases}$$

$$v_{21}(p_1) = \begin{cases} -1.8, & |p_1(t)| < 1, \\ -1.4, & |p_1(t)| > 1, \end{cases} \quad v_{22}(p_2) = \begin{cases} -1.5, & |p_2(t)| < 1, \\ -1.6, & |p_2(t)| > 1, \end{cases}$$

$$v_{23}(p_3) = \begin{cases} 0.2, & |p_3(t)| < 1, \\ 0.3, & |p_3(t)| > 1, \end{cases} \quad v_{31}(p_1) = \begin{cases} -2.3, & |p_1(t)| < 1, \\ -2.1, & |p_1(t)| > 1, \end{cases}$$

$$v_{32}(p_2) = \begin{cases} 3, & |p_2(t)| < 1, \\ 2, & |p_2(t)| > 1, \end{cases} \quad v_{33}(p_3) = \begin{cases} -1.1, & |p_3(t)| < 1, \\ -1.3, & |p_3(t)| > 1, \end{cases}$$

$\eta = 0.98$, $\tau_1 = 0.2$, $\tau_2 = 0.3$, $\tau_3 = 0.4$, $w_k = 1$, $I_1(t) = 0.15\ sint$, $I_2(t) = 0.2\ cost$, $I_3(t) = 0.3\ cost$,

$$\Delta\overline{u}_{kj} = \begin{bmatrix} -0.2\ sint & 0.3\ cost & 0.3\ sint \\ 0 & 0.2\ sint & 0 \\ 0.06\ cost & 0.3\ sint & 0.1\ sint \end{bmatrix} \text{ and } \Delta\overline{v}_{kj} = \begin{bmatrix} 0.03\ cost & -0.1\ sint & 0.2\ sint \\ 0.04\ cost & 0.3\ cost & 0.2\ cost \\ 0 & -0.1\ sint & 0.5\ cost \end{bmatrix}.$$

According to drive neural networks (52), the response neural networks can be given as

$$\begin{cases} {}^cD_t^\eta q_1(t) = -w_1 q_1(t) + \sum\limits_{j=1}^{3} \Big(u_{1j}(q_j) + \Delta\overline{u}_{1j}\Big)\tanh(q_j(t)) + \sum\limits_{j=1}^{3} \Big(v_{1j}(q_j) + \Delta\overline{v}_{1j}\Big) \\ \qquad \times \tanh(q_j(t-\tau_j)) + I_1(t) + U_1(t), \\ {}^cD_t^\eta q_2(t) = -w_2 q_2(t) + \sum\limits_{j=1}^{3} \Big(u_{2j}(q_j) + \Delta\overline{u}_{2j}\Big)\tanh(q_j(t)) + \sum\limits_{j=1}^{3} \Big(v_{2j}(q_j) + \Delta\overline{v}_{2j}\Big) \\ \qquad \times \tanh(q_j(t-\tau_j)) + I_2(t) + U_2(t), \\ {}^cD_t^\eta q_3(t) = -w_3 q_3(t) + \sum\limits_{j=1}^{3} \Big(u_{3j}(q_j) + \Delta\overline{u}_{3j}\Big)\tanh(q_j(t)) + \sum\limits_{j=1}^{3} \Big(v_{3j}(q_j) + \Delta\overline{v}_{3j}\Big) \\ \qquad \times \tanh(q_j(t-\tau_j)) + I_3(t) + U_3(t), \end{cases} \tag{53}$$

where

$$u_{11}(q_1) = \begin{cases} 3.2, & |q_1(t)| < 1, \\ 3.1, & |q_1(t)| > 1, \end{cases} \quad u_{12}(q_2) = \begin{cases} -2, & |q_2(t)| < 1, \\ -1.1, & |q_2(t)| > 1, \end{cases}$$

$$u_{13}(q_3) = \begin{cases} -3.1, & |q_3(t)| < 1, \\ -4.1, & |q_3(t)| > 1, \end{cases} \quad u_{21}(q_1) = \begin{cases} 1, & |q_1(t)| < 1, \\ 0.9, & |q_1(t)| > 1, \end{cases}$$

$$u_{22}(q_2) = \begin{cases} 2, & |q_2(t)| < 1, \\ 1.9 + \frac{\pi}{4}, & |q_2(t)| > 1, \end{cases} \quad u_{23}(q_3) = \begin{cases} -0.9, & |q_3(t)| < 1, \\ -5, & |q_3(t)| > 1, \end{cases}$$

$$u_{31}(q_1) = \begin{cases} 3.5, & |q_1(t)| < 1, \\ 6.1, & |q_1(t)| > 1, \end{cases} \quad u_{32}(q_2) = \begin{cases} -1.2, & |q_2(t)| < 1, \\ -1.6, & |q_2(t)| > 1, \end{cases}$$

$$u_{33}(q_3) = \begin{cases} -2, & |q_3(t)| < 1, \\ -1.1, & |q_3(t)| > 1, \end{cases} \quad v_{11}(q_1) = \begin{cases} -2.2, & |q_1(t)| < 1, \\ -2.2, & |q_1(t)| > 1, \end{cases}$$

$$v_{12}(q_2) = \begin{cases} 0.15, & |q_2(t)| < 1, \\ 0.23, & |q_2(t)| > 1, \end{cases} \quad v_{13}(q_3) = \begin{cases} -0.85, & |q_3(t)| < 1, \\ 0.9, & |q_3(t)| > 1, \end{cases}$$

$$v_{21}(q_1) = \begin{cases} -1.8, & |q_1(t)| < 1, \\ -1.4, & |q_1(t)| > 1, \end{cases} \quad v_{22}(q_2) = \begin{cases} -1.5, & |q_2(t)| < 1, \\ -1.6, & |q_2(t)| > 1, \end{cases}$$

$$v_{23}(q_3) = \begin{cases} 0.2, & |q_3(t)| < 1, \\ 0.3, & |q_3(t)| > 1, \end{cases} \quad v_{31}(q_1) = \begin{cases} -2.3, & |q_1(t)| < 1, \\ -2.1, & |q_1(t)| > 1, \end{cases}$$

$$v_{32}(q_2) = \begin{cases} 3, & |q_2(t)| < 1, \\ 2, & |q_2(t)| > 1, \end{cases} \quad v_{33}(q_3) = \begin{cases} -1.1, & |q_3(t)| < 1, \\ -1.3, & |q_3(t)| > 1, \end{cases}$$

and other network parameters have the same values as system (52). Based on Definition 3 and Assumption 2, choosing the time-varying projective scaling matrix as $\Xi(t) = \begin{bmatrix} 1 - 0.02\sin t & 0.5\sin t & -\sin t \\ -\cos t & -0.03\cos t & -0.01\cos t \\ 1.2 - 0.07\cos t & 2\cos t & -\sin 3t \end{bmatrix}$, then one can obtain the error functions of TFMPS as $z_1 = q_1 - [p_1(1 - 0.02\sin t) + 0.5p_2\sin t - p_3\sin t]$, $z_2 = q_2 - [-p_1\cos t - 0.03p_2\cos t - 0.01p_3\cos t]$, and $z_3 = q_3 - [p_1(1.2 - 0.07\cos t) + 2p_2\cos t - p_3\sin 3t]$.

To achieve the TFMPS between Caputo FOUMNNs (52) and (53), feedback control strengths d_k and d_k^τ in (13) can be selected as $d_1 = d_2 = d_3 = 25$, $d_1^\tau = d_2^\tau = d_3^\tau = 1$. The impulsive control strength and impulsive intervals can be chosen as $\omega_k = -0.21$ and $t_\sigma - t_{\sigma-1} = 0.15$, respectively. The Lipschitz constants are set as $\tilde{\phi}_j = \tilde{\varphi}_j = 1, j = 1, 2, 3$, and one can verify that Assumption 1 is valid. Chose parameter $\gamma = 0.8$, and then simple calculation shows that $\beta_1 = \sum_{k=1}^{3} \tilde{\varphi}_1(v_{k1}^+ + \varrho_{k1}) + |d_1^\tau| = 7.37$, $\beta_2 = \sum_{k=1}^{3} \tilde{\varphi}_2(v_{k2}^+ + \varrho_{k2}) + |d_2^\tau| = 6.33$, $\beta_3 = \sum_{k=1}^{3} \tilde{\varphi}_3(v_{k3}^+ + \varrho_{k3}) + |d_3^\tau| = 4.4$, $\underline{\beta} = \min_{1\le k\le n}\Big[2(w_k + d_k) - |d_k^\tau| - \sum_{j=1}^{3} \tilde{\phi}_j(u_{kj}^+ + \rho_{kj}) - \sum_{j=1}^{3} \tilde{\phi}_k(u_{jk}^+ + \rho_{jk}) - \sum_{j=1}^{3} \tilde{\varphi}_j(v_{kj}^+ + \varrho_{kj})\Big] = 22.14$, $\sum_{j=1}^{3} \beta_j - \underline{\beta}\sin\frac{\eta\pi}{2} = -5.04 < 0$, and $\begin{bmatrix} -0.8I_3 & \Xi_3^T \\ \Xi_3 & -I_3 \end{bmatrix} \le 0$. Consequently, the calculation results indicate that all parameters meet the requirements of Theorem 1.

The initial values of memristive network systems (52) and (53) are generated randomly in the interval $[-5, 5]$. By utilizing Matlab software, the state trajectories and error functions for systems (52) and (53) are shown in Figure 3. As one can see in Figure 3a–c, under the influence of scale factors, the red, blue, and pink curves representing state trajectories in the controlled drive-response memristive systems gradually overlap with time evolution. Furthermore, as shown in Figure 3d,f, three colored error curves of different dimensions gradually approach zero, indicating the correctness of the obtained theorem and the effectiveness of the mixed control scheme proposed in this article.

Remark 10. *Our control techniques and synchronization results are still effective when uncertainty factors are not considered, as shown in Corollary 1. Under this case, our network model degenerates into [30–32]. Therefore, the results of this article are more generalized than existing results [30–32].*

Remark 11. *The derived results in our theorem and corollary are also applicable for parameter $\eta = 1$, i.e., the mixed impulsive feedback control method is still suitable for the corresponding integer-order memristor-based systems, such as [18,20].*

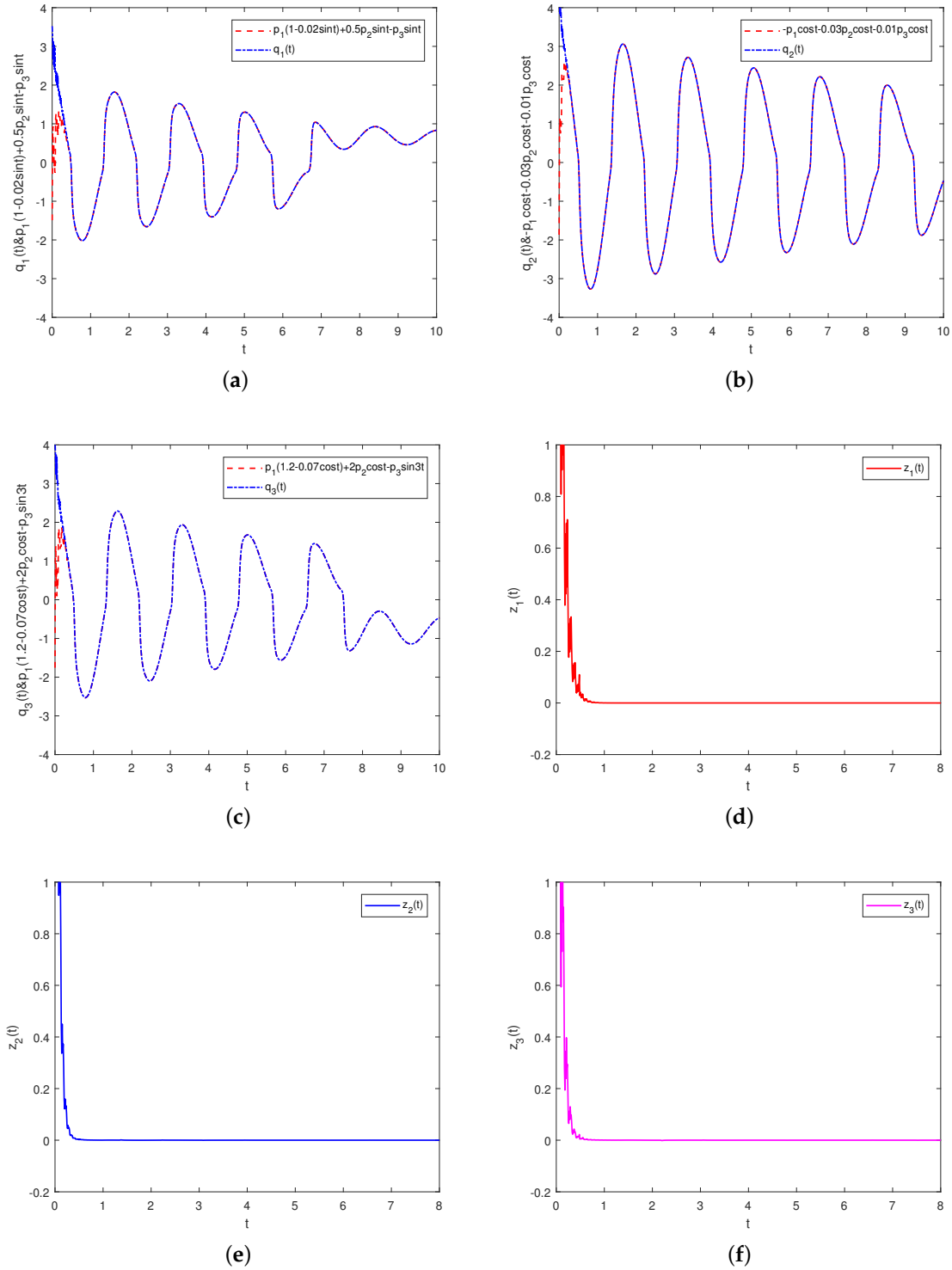

Figure 3. The state trajectories and error functions in systems (52) and (53) with control intensities $d_k = 25$ in Example 2. (**a**) $q_1(t)\&p_1(1-0.02\sin t)+0.5p_2\sin t-p_3\sin t$; (**b**) $q_2(t)\&-p_1\cos t-0.03p_2\cos t-0.01p_3\cos t$; (**c**) $q_3(t)\&p_1(1.2-0.07\cos t)+2p_2\cos t-p_3\sin 3t$; (**d**) $z_1(t)$; (**e**) $z_2(t)$; (**f**) $z_3(t)$.

5. Conclusions

In this article, the nontraditional TFMPS pattern for FOUMNNs with multiple delays is investigated by utilizing mixed impulsive feedback control. The control scheme takes into account both the open-loop feedback term and the impulse term, utilizing not only the state information of the delayed intervals but also the sampling information of the

impulse moments. Unlike the pure impulse control method, the impulse interval in this paper cannot be restricted by time delays. The adjustability of fractional order and time-varying unpredictability of elements in function projective matrices can improve communication security and provide better application prospects for network confidential communication. Based on the proposed impulsive comparison theorem, stability theory, and linear matrix inequality technique, novel synchronization criteria relying on impulsive strengths, feedback strengths, uncertain boundaries, and fractional order are derived for considering FOUMNNs. Using event-triggering strategies to select impulse instants, we will study the TFMPS pattern for the variable-order memristive systems in the future.

Author Contributions: Conceptualization, K.S., H.W. and H.F.; Methodology, H.W. and K.S.; software, H.F. and Y.R.; Writing—original draft, H.F., Y.R. and K.S.; Writing—review and editing, H.F. and H.W. All authors have read and agreed to the published version of the manuscript.

Funding: The first author was partially supported by the Open Foundation of Engineering Research Center of Big Data Application in Private Health Medicine, Fujian Province University under Grant (MKF202201). The third author was partially supported by the Sichuan Science and Technology Program under Grant (21YYJC0469), the Key R&D Projects of Sichuan Provincial Department of Science and Technology under Grant (2023YFG0287), and the Program of Science and Technology of Sichuan Province of China under Grant (2021ZYD0012). The fourth author was partially supported by the Introducing Talent Projects of Putian University (Seedling Fund) under Grant (2019110), the Natural Science Foundation of Fujian Province under Grant (2023J011015), and the APC was funded by (2023J011015).

Data Availability Statement: Data are contained within the article.

Conflicts of Interest: The authors declare no conflicts of interest.

References

1. Pham, H.; Warin, X. Mean-field neural networks: Learning mappings on Wasserstein space. *Neural Netw.* **2023**, *168*, 380–393. [CrossRef] [PubMed]
2. Tang, Z.; Xuan, D.L.; Park, J.H.; Wang, Y.; Feng, J.W. Impulsive effects based distributed synchronization of heterogeneous coupled neural networks. *IEEE Trans. Netw. Sci. Eng.* **2021**, *8*, 498–510. [CrossRef]
3. Jiang, C.H.; Tang, Z.; Park, J.H.; Xiong, N.N. Matrix measure-based projective synchronization on coupled neural networks with clustering trees. *IEEE Trans. Cybern.* **2023**, *53*, 1222–1234. [CrossRef] [PubMed]
4. Zhong, Q.S.; Han, S.; Shi, K.B.; Zhong, S.M.; Kwon, O.-M. Co-design of adaptive memory event-triggered mechanism and aperiodic intermittent controller for nonlinear networked control systems. *IEEE Trans. Circuits Syst. II Express Briefs.* **2022**, *69*, 4979–4983. [CrossRef]
5. Shi, K.B.; Cai, X.; She, K.; Wen, S.P.; Zhong, S.M.; Park, P.; Kwon, O.-M. Stability analysis and security-based event-triggered mechanism design for T-S fuzzy NCS with traffic congestion via DoS attack and its application. *IEEE Trans. Fuzzy Syst.* **2023**, *31*, 3639–3651. [CrossRef]
6. Kong, F.C.; Zhu, Q.X.; Huang, T.W. New fixed-time stability lemmas and applications to the discontinuous fuzzy inertial neural networks. *IEEE Trans. Fuzzy Syst.* **2021**, *29*, 3711–3722. [CrossRef]
7. Liu, P.; Zeng, Z.; Wang, J. Multiple Mittag-Leffler stability of fractional-order recurrent neural networks. *IEEE Trans. Syst. Man Cybern. Syst.* **2017**, *47*, 2279–2288. [CrossRef]
8. Tang, C.; Liu, J.X. The equivalence conditions of optimal feedback control-strategy operators for zero-sum linear quadratic stochastic differential game with random coefficients. *Symmetry* **2023**, *15*, 1726. [CrossRef]
9. Cai, J.Y.; Yi, C.B.; Wu, Y.; Liu, D.Q.; Zhong, D.G. Leader-following consensus of nonlinear singular switched multi-agent systems via sliding mode control. *Asian J. Control.* **2024**, *26*, 1–14. [CrossRef]
10. Adhikari, S.P.; Yang, C.; Kim, H.; Chua, L.O. Memristor bridge synapse-based neural network and its learning. *IEEE Trans. Neural Netw. Learn. Syst.* **2012**, *23*, 1426–1435. [CrossRef]
11. Dou, H.; Shen, F.; Zhao, J.; Mu, X.Y. Understanding neural network through neuron level visualization. *Neural Netw.* **2023**, *168*, 484–495. [CrossRef] [PubMed]
12. Zhou, C.; Wang, C.H.; Yao, W.; Lin, H.R. Observer-based synchronization of memristive neural networks under dos attacks and actuator saturation and its application to image encryption. *Appl. Math. Comput.* **2022**, *425*, 127080. [CrossRef]
13. Cheng, J.; Lin, A.; Cao, J.D.; Qiu, J.L.; Qi, W.H. Protocol-based fault detection for discrete-time memristive neural networks with effect. *Inf. Sci.* **2022**, *615*, 118–135. [CrossRef]

14. Wang, X.; Park, J.H.; Zhong, S.M.; Yang, H.L.A switched operation approach to sampled-data control stabilization of fuzzy memristive neural networks with time-varying delay. *IEEE Trans. Neural Netw. Learn. Syst.* **2020**, *31*, 891–900. [CrossRef] [PubMed]
15. Wang, F.; Yang, Y.Q. Intermittent synchronization of fractional order coupled nonlinear systems based on a new differential inequality. *Physica A* **2018**, *512*, 142–152. [CrossRef]
16. Wang, F.; Zheng, Z.W.; Yang, Y.Q. Quasi-synchronization of heterogenous fractional-order dynamical networks with time-varying delay via distributed impulsive control. *Chaos Sol. Fract.* **2021**, *142*, 110465. [CrossRef]
17. Bao, H.B.; Park, J.H.; Cao, J.D. Exponential synchronization of coupled stochastic memristor-based neural networks with time-varying probabilistic delay coupling and impulsive delay. *IEEE Trans. Neural Netw. Learn. Syst.* **2016**, *27*, 190–201. [CrossRef] [PubMed]
18. Li, X.F.; Zhang, W.B.; Fang, J.A.; Li, H.Y. Finite-time synchronization of memristive neural networks with discontinuous activation functions and mixed time-varying delays. *Neurocomputing* **2019**, *340*, 99–109. [CrossRef]
19. Yu, T.H.; Cao, J.D.; Rutkowski, L.; Luo, Y.P. Finite-time synchronization of complex-valued memristive-based neural networks via hybrid controls. *IEEE Trans. Neural Netw. Learn. Syst.* **2022**.*33*, 3938–3947. [CrossRef]
20. Alsaedi, A.; Cao, J.D.; Ahmad, B.; Alshehri, A.; Tan, X.G. Synchronization of master-slave memristive neural networks via fuzzy output-based adaptive strategy. *Chaos Sol. Fract.* **2022**, *158*, 112095. [CrossRef]
21. Fu, Q.H.; Zhong, S.M.; Jiang, W.B.; Xie, W.Q. Projective synchronization of fuzzy memristive neural networks with pinning impulsive control. *J. Frankl. Inst.* **2020**, *375*, 10387–10409. [CrossRef]
22. Wang, F.; Zheng, Z.W. Quasi-projective synchronization of fractional order chaotic systems under input saturation. *Physica A* **2019**, *534*, 122132. [CrossRef]
23. Chen, L.P.; Cao, J.D.; Wu, R.C.; Machado, J.A.T.; Lopes, A.M.; Yang, H.J. Stability and synchronization of fractional-order memristive neural networks with multiple delays. *Neural Netw.* **2017**, *94*, 76–85 [CrossRef] [PubMed]
24. Jarad, F.; Abdeljawad, T.; Alzabut, J. Generalized fractional derivatives generated by a class of local proportional derivatives. *Eur. Phys. J. Spec. Top.* **2017**, *226*, 3457–3471. [CrossRef]
25. Makhlouf, A.B.; Mchiri, L.; Srivastava, H.M. Some existence and uniqueness results for a class of proportional Liouville-Caputo fractional stochastic differential equations. *Bull. Sci. Math.* **2023**, *189*, 103349. [CrossRef]
26. Gu, Y.J.; Wang, H.; Yu, Y.G. Synchronization for commensurate Riemann-Liouville fractional-order memristor-based neural networks with unknown parameters. *J. Frankl. Inst.* **2020**, *357*, 8870–8898. [CrossRef]
27. Chen, J.J.; Zeng, Z.G.; Jiang, P. Global Mittag-Leffler stability of coupled system of fractional-order differential equations on networks. *Neural Netw.* **2014**, *51*, 1–8. [CrossRef] [PubMed]
28. Li, X.M.; Liu, X.G.; Wang, F.X. Anti-synchronization of fractional-order complex-valued neural networks with a leakage delay and time-varying delays. *Chaos Sol. Fract.* **2023**, *174*, 113754. [CrossRef]
29. Yang, X.J.; Li, C.D.; Huang, T.W.; Song, Q.K.; Huang, J.J. Synchronization of fractional-order memristor-based complex-valued neural networks with uncertain parameters and time delays. *Chaos Sol. Fract.* **2018**, *110*, 105–123. [CrossRef]
30. Liu, S.X.; Yu, Y.G.; Zhang, S. Robust synchronization of memristor-based fractional-order Hopfield neural networks with parameter uncertainties. *Neural Comput. Appl.* **2019**, *31*, 3533–3542. [CrossRef]
31. Peng, L.B.; Li, X.F.; Bi, D.J.; Xie, X.; Xie, Y.L. Pinning multisynchronization of delayed fractional-order memristor-based neural networks with nonlinear coupling and almost-periodic perturbations. *Neural Netw.* **2021**, *144*, 372–383. [CrossRef]
32. Bao, H.B.; Cao, J.D. Projective synchronization of fractional-order memristor-based neural networks. *Neural Netw.* **2015**, *63*, 1–9. [CrossRef]
33. Wang, F.; Yang, Y.Q.; Zhang, L.Z. Projective synchronization of fractional-order memristor-based neural networks with switching jumps mismatch. *Physica A* **2017**, *471*, 402–415.
34. Velmurugan, G.; Rakkiyappan, R. Hybrid projective synchronization of fractional-order memristor-based neural networks with time delays. *Nonlin. Dyn.* **2016**, *83*, 419–432. [CrossRef]
35. Gu, Y.J.; Yu, Y.G.; Wang, H. Projective synchronization for fractional-order memristor-based neural networks with time delays. *Neural Comput. Appl.* **2019**, *31*, 6039–6054. [CrossRef]
36. Song, S.; Song, X.N.; Balsera, I.T. Mixed H_∞ and passive projective synchronization for fractional-order memristor-based neural networks with time delays via adaptive sliding mode control. *Neural Process. Lett.* **2018**, *47*, 443–462. [CrossRef]
37. Yang, S.; Hu, C.; Yu, J.; Jiang, H.J. Projective synchronization in finite-time for fully quaternion-valued memristive networks with fractional-order. *Chaos Sol. Fract.* **2021**, *147*, 110911. [CrossRef]
38. Qin, X.L.; Wang, C.; Li, L.X.; Peng, H.P.; Yang, Y.X.; Ye, L. Finite-time modified projective synchronization of memristor-based neural networks with multi-links and leakage delay. *Chaos Sol. Fract.* **2018**, *116*, 302–315. [CrossRef]
39. Ding, Z.X.; Chen, C.; Wen, S.P.; Li, S.; Wang, L.H. Lag projective synchronization of nonidentical fractional delayed memristive neural networks. *Neurocomputing* **2022**, *469*, 138–150. [CrossRef]
40. Ding, D.W.; Yao, X.L.; Zhang, H.W. Complex projective synchronization of fractional-order complex-valued memristive neural networks with multiple delays. *Neural Process. Lett.* **2020**, *51*, 325–345. [CrossRef]
41. He, J.M.; Chen, F.Q.; Lei, T.F.; Bi, Q.S. Global adaptive matrix-projective synchronization of delayed fractional order competitive neural networks with different time scales. *Neural Comput. Appl.* **2020**, *32*, 12813–12826. [CrossRef]

42. Cao, Y.Y.; Jiang, W.J.; Wang, J.H. Anti-synchronization of delayed memristive neural networks with leakage term and reaction-diffusion terms. *Knowl. Based Syst.* **2021**,*233*, 107539. [CrossRef]
43. Wang, H.; Yu, Y.G.; Wen, G.G. Global stability analysis of fractional-order Hopfield neural networks with time delay. *Neurocomputing* **2015**, *154*, 15–23. [CrossRef]
44. Aguila-Camacho, N.; Duarte-Mermoud, M.; Gallegos, J. Lyapunov functions for fractional order systems. *Commun. Nonlinear Sci. Numer. Simul.* **2014**, *19*, 2951–2957. [CrossRef]
45. Boyd, S.; Ghaoui, L.E.; Feron, E.; Balakrishnan, V. *Linear Matrix Inequalities in System and Control Theory*; SIAM: Philadelphia, PA, USA, 1994.
46. Bhalekar, S.; Gejji, V. A predictor-corrector scheme for solving nonlinear delay differential equations of fractional order. *J. Fract. Calc. Appl.* **2011**, *1*, 1–9.